



Project Number: <D50-0207>

Effects of Trailing Edge Notches on Micro Air Vehicle Performance

A Major Qualifying Project Report

Submitted to the Faculty of the

WORCESTER POLYTECHNIC INSTITUTE

in partial fulfillment of the requirements for the

Degree of Bachelor of Science

in Mechanical Engineering and Aerospace Engineering

by

Nicholas Cubin (ME/Aero), Rob DeSignore (Aero), Rich McCann (Aero)

Date: April 24, 2007

Approved:

Prof. David Olinger, Major Advisor

Prof. Islam Hussein, Co-Advisor

Acknowledgments

We would like to thank the following people for their contributions to this MQP:

Professor David Olinger
Professor Islam Hussein

We would also like to thank Mr. Anthony McCann and Mr. James McCann, whose expertise and material support were instrumental in getting our MAV's airborne.

Table of Contents

Acknowledgments.....	2
Table of Contents.....	3
Table of Figures.....	4
Abstract.....	5
Section 1: Introduction.....	6
1.1 Background.....	6
1.2 Previous Research.....	10
1.3 Project Objectives.....	15
Section 2: Methodology.....	16
2.1: Design of the Force Balance.....	16
2.1.1: Base.....	16
2.1.2: Stand and Sting.....	19
2.1.3: Final Design.....	21
2.2: Wind Tunnel Testing.....	22
2.2.1: Setup.....	22
2.2.2: Measuring Forces.....	23
2.2.3: Drag Calibration.....	25
2.2.4: Sting Drag Measurements.....	27
2.2.5: Data Collection.....	28
2.2.6: Induced Drag.....	30
2.2.7: Excel Data Sheet.....	31
2.2.8: Error Bars.....	36
2.3: Micro-Air Vehicle Testing.....	38
2.3.1 MAV Design.....	38
2.3.2 MAV Testing.....	40
Section 3: Results and Analysis.....	44
3.1: 3-D Test Results.....	44
3.1.1: C_L vs. α	44
3.1.2: L/D vs. α	48
3.2: 2-D Test Results.....	51
3.2.1: C_L vs. α	51
3.2.2: L/D vs. α	51
3.3: Induced Drag and Span Efficiency Factor.....	54
3.4: Flight Test Results.....	57
Section 4: Conclusions.....	58
References.....	59
Appendix A – Force Balance Construction.....	60
A.1: Base Construction.....	60
A.2: Steel Shim Construction.....	61
Appendix B – Stand and Sting CAD Design.....	62

Table of Figures

Figure 1: MAV - WASP [10].....	8
Figure 2: MAV System Integration [1].....	8
Figure 3: Minimization of MAV Propulsion Power [1]	9
Figure 4: Experimental Wing Models [3].....	10
Figure 5: Design of Airfoil Containing Wing Tips [6].....	11
Figure 6: Comparison of Lift-to-Drag Ratios for Airfoils with Varying Notch Locations [9].....	12
Figure 7: Comparison of Lift-to-Drag Ratios for Airfoils with Varying Notch Size [9]	13
Figure 8: Optimal Notched Airfoil vs. Unnotched Airfoil [9].....	14
Figure 9: Base - Side A.....	16
Figure 10: Base – Front.....	17
Figure 11: Base – Back.....	17
Figure 12: Base - Side B.....	17
Figure 13: Lift/Drag/Moments Diagram.....	18
Figure 14: Base - Top	19
Figure 15: Stand - Gear Setup [9].....	20
Figure 16: Sting [9].....	20
Figure 17: Force Balance [9]	21
Figure 18: Flat-Plate Attached to Sting	23
Figure 19: Digital Scales.....	24
Figure 20: Drag Calibration Setup.....	25
Figure 21: Drag Calibration Curve.....	26
Figure 22: Force Balance Stand with Drag Shield.....	28
Figure 23: Scale Readings at Two Different Times.....	30
Figure 24: 2-D Wing Test Setup.....	31
Figure 25: Drag Calibration Sheet.....	32
Figure 26: Notched/Unnotched Data Sheet	35
Figure 27: 2001 MAV.....	38
Figure 28: Redesigned MAV - 2007.....	40
Figure 29: Notches Cut into Elevons.....	42
Figure 30: 3-D Coefficient of Lift vs. AOA (radians).....	44
Figure 31: 3-D Coefficient of Lift vs. AOA (degrees)	45
Figure 32: 3-D Coefficient of Lift vs. Angle of Attack Comparison.....	45
Figure 33: 3-D Coefficient of Lift vs. Angle of Attack compared to Lifting Line Theory	46
Figure 34: 3-D Coefficient of Lift vs. Angle of Attack for Notched/Unnotched–Re=46,600.....	47
Figure 35: 3-D Coefficient of Lift vs. Angle of Attack for Notched/Unnotched–Re=73,200.....	47
Figure 36: 3-D Coefficient of Lift vs. Angle of Attack for Notched/Unnotched–Re=102,600....	48
Figure 37: Notched/Unnotched Lift to Drag Comparison	49
Figure 38: Lift to Drag Comparison to Previous Data.....	50
Figure 39: 2-D Coefficient of Lift vs. Angle of Attack	51
Figure 40: 2-D Lift to Drag Ratio	52
Figure 41: Drag Force 3-D vs. 2-D – Re=102,500	52
Figure 42: 3-D Coefficient of Drag vs. Square of Coefficient of Lift	55
Figure 43: 2-D Coefficient of Drag vs. Square of Coefficient of Lift	55
Figure 44: Sting [8].....	62
Figure 45: Stand and Sting [8].....	62

Abstract

Over the past decade there has been a surge in interest in Micro Air Vehicles (MAV) for surveillance and reconnaissance purposes. This has led to a revitalized interest in aerodynamics in the low Reynolds number (50,000-250,000) flight regime. Several studies conducted at WPI have suggested that peaks in the span-wise lift distribution, of flat plate wings, exist at 60% of the wing half-span resulting in a non-ideal lift profile. This project has sought to determine whether or not this lift profile can be “reshaped” through the use of trailing edge notches to reduce local planform area, thereby reducing the local lift, in order to create an ideal, elliptical lift profile across the wing. A previous MQP (Blanchard, DeFusco, and Donoghue, 2006) has suggested that these trailing edge notches may increase the lift to drag ratio of MAV wings. In our study we have observed the following:

- Equilateral triangular trailing edge notches (1.76% of the planform area) placed at the suggested 60% half-span had little noticeable effect in improving lift to drag ratios
- Trailing edge notches reduced the induced drag on $AR = 1$ wings by $\sim 3\%$

Section 1: Introduction

1.1 Background

Uninhabited Aerial Vehicles (UAV) are becoming a major focus of both military and civilian aviation. They are piloted either remotely by a human operator or by an onboard flight computer and as a result, allow aircraft to operate in hazardous areas that might have been too dangerous for an aircraft with an onboard crew to enter. This includes military reconnaissance, detecting biological and nuclear materials, and targeting enemy troops.

Although development of UAV's have become quite prevalent in the past 10 years, the interest in UAV's began as far back as the 1960's with the creation of the Model 147 Firebee. The Firebee's primary mission was to conduct surveillance over foreign countries and had a wing span of 32 ft and a total length of 30 ft while weighing just over 3,800 pounds. Currently, the most used and most successful UAV in operation is the RQ-4 Global Hawk. The Global Hawk has a wing span of 120 ft, a length of 44 ft and weighs in at 26,700 pounds. As can be seen by the technical specifications of the two aircraft, for the past 40 years larger UAV's seemed to be the popular choice. It wasn't until 1990 when the RAND Corporation released a study where they investigated the use of microsystems and MIT did research on mirco-flyers, did the organizations interested in UAV's start to think small. In 1995, DARPA (Defense Advanced Research Projects Agency) conducted a workshop on the feasibility of smaller UAV's and determined that the technology was available and the characteristics and capabilities of small UAV's would be of great use to them in present day warfare (McMichael and Francis [1]).

With the development of smaller UAV's comes a reduction of production cost as well as an increase in versatility. The Global Hawk has a total cost of approximately \$15 million to manufacture and is limited to high altitude reconnaissance. The Predator and the Desert Hawk, two much smaller UAV's, are significantly cheaper and provides more ground-level capabilities. The Predator has the ability to be equipped with anti-tank missiles and the Desert Hawk can perform pre-programmed scouting missions on enemy bases. DARPA's final goal however is to create small UAV's, 15 to 25cm, called Micro Aerial Vehicles (MAV).

The missions that an MAV would potentially perform range from target surveillance to contaminate sensing and short range terrain mapping. Another potential application is situational awareness in urban combat, where one of the oldest questions for any soldier is, what is over that

next hill? The hopes for MAV's are that they will be able to answer that question with a capacity to deliver short range tactical intelligence directly to small ground units in the field.

Currently most UAV's require support equipment that does not allow leaders of small units direct access to the intelligence they are capable of gathering. The military is interested in the development of an aircraft that can be carried and employed in combat by any soldier. MAV's offer the ability to sneak in close to an enemy and shadow him without being observed thanks to the MAV's size and low noise signature. These two traits combined with superior maneuverability also make an MAV the perfect surveillance tool for the urban combat environment. MAV's can not only maneuver between buildings but could also enter the buildings and gather intelligence. Contaminate sensing is another mission well suited to MAV's. These small vehicles can easily fly sensor packages into a perceived threat area and provide data on the extent of a potential chemical, biological, or radiological contamination without risk to human life. This is especially important for urban and indoor operations where larger UAV's or ground-based robots may not be able to operate.

Civilian operators are also interested in the capabilities of MAV's. Law enforcement and security companies are interested in MAV's for many of the same reasons as the military. Micro air vehicles are less likely to be spotted by criminals and could follow them inside buildings and provide law enforcement officers the ability to gather intelligence and evidence. Other possible civilian uses include traffic monitoring, border surveillance, fire and rescue operations, forestry, wildlife surveys, power-line inspection and real-estate aerial photography.

According to Goebel [2], DARPA's original goal for MAV's was "to develop a microdrone whose largest dimension was no more than 15 centimeters (6 inches); would carry a day-night imager; have an endurance of about two hours; and be very low cost. It would operate with a high degree of autonomy to be used in the squad-level combat environment. MAV's capable of hovering and vertical flight would be used to scout out buildings for urban combat and counter terrorist operations. A MAV could be included in a pilot's survival kit. A downed pilot could use it to keep a lookout for enemy search parties, or relay communications to search and rescue units." DARPA's lofty goals have been met with many challenges. MAV's, while small in size, operate at speeds of about 10 m/s and low Reynolds numbers between 30,000 and 200,000. Torres and Mueller [3] concluded that at this size and speed, conventional aerodynamic theories applied to larger aircraft breakdown. Furthermore, there has been very little research

conducted on aircraft with this type of flight regime and due this lack of research MAV's are still quite unpredictable and unreliable.



Figure 1: MAV - WASP [10]

Obviously aerodynamic analysis is critical to the success of MAV's however there are many other factors that must be studied if the original DARPA goals are to be reached. One challenge that must be overcome involves integrating the hardware into the MAV. As can be seen in Figure 2, there are a great deal of systems that must be placed somewhere on the aircraft and at 15 cm there is very little room to store them all.

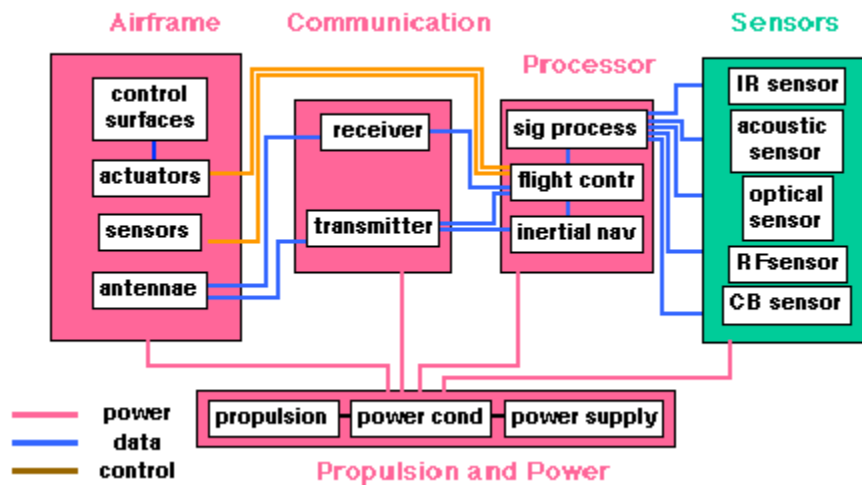


Figure 2: MAV System Integration [1]

One encouraging element of hardware integration entails the use of microelectronics, which continues to make strides everyday, however McMichael and Francis take it even farther and propose making the physical components serve multiple purposes. One example has the wings serve as an antenna or as sensor apertures.

Another challenge is producing stable flight. Even the smallest forces can disrupt the flight path of MAV's where inertia is almost nonexistent. This has led to a fair amount of research comparing MAV's to animals in nature. The ideas of flapping wings and low aspect ratios have come from looking at insects such as the butterfly.

Small scale propulsion systems are another aspect of concern. McMichael and Francis look at the power equation for propeller driven aircraft (seen in Figure 3) and establish what they feel needs to be done to maximizing the propulsion.

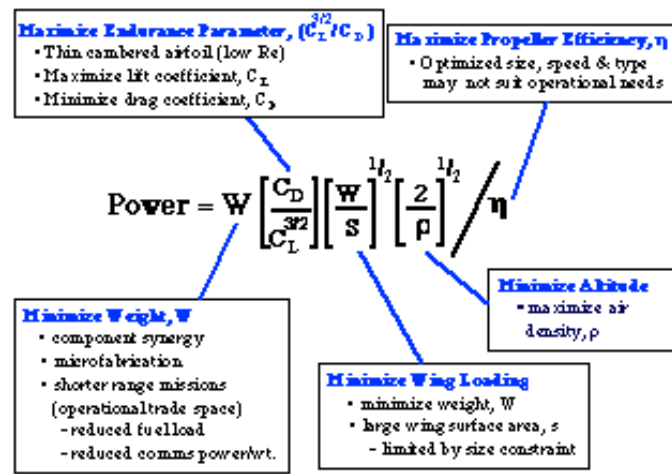


Figure 3: Minimization of MAV Propulsion Power [1]

One challenge that arises from the equation seen in Figure 3 is improving the lift to drag ratio. MAV lift to drag ratios is typically 25-35% of those of a conventional aircraft and finding a way to maximize the ratio at a low Reynolds number is critical. Research involving notches on the trailing edge of wings will help to accomplish this and be discussed later on in this report. Among the issues with hardware integration, flight stabilization, propulsion, and wing design are the topics of navigation, communication, increased payloads, aircraft fortitude, and production costs.

Despite the difficulties, MAV researchers continue to draw funding from many sources. In 2004, the Department of Defense set aside \$1 billion for all UAV spending with MAV spending (a subdivision of the DOD UAV budget) growing each year since 2000.

The next section will provide an overview of some of the research that has been conducted on MAV's and more specifically on MAV wings. This will include wing geometry and also aerodynamic analysis at low Reynolds numbers.

1.2 Previous Research

As discussed in the previous section, DARPA is seeking very specific parameters for its ideal MAV design. However, as Torres and Mueller [3] have described, the current aerodynamic research conducted on MAV's is very limited and still does not allow for the design and development of MAV's with DARPA's desired capabilities. This section will discuss some of the research that has been done on MAV wings and what this means for future research.

In terms of the aspect ratio of MAV wings, Torres and Mueller have conducted research in the area by performing wind tunnel tests on flat plates with various planform shapes and aspect ratios ranging from .5 to 2. The results concluded that lift curves become nonlinear as the aspect ratio decreases, the angle of attack of stall increases as aspect ratios decrease, and for an aspect ratio equivalent to one or less, rectangular and inverse Zimmerman planforms are most efficient. Figure 4 below presents the geometry Torres and Mueller used for their flat plates during testing. Overall, the testing indicated that low aspect ratios close to one produce the most promising results.





























AR	Rectangular	Zimmerman	Inv. Zimmerman	Elliptical
0.50				
0.75				
1.00				
1.25				
1.50				
1.75				
2.00				

Figure 4: Experimental Wing Models [3]

Null and Shkarayev [4] followed up Torres and Mueller's research with tests focusing on the camber of MAV wings. Four wind-tunnel models were built with 3, 6, 9, and 12% cambers based upon the S5010-TOP24C-REF thin, cambered-plate airfoil. They were tested at angles of attack ranging from 0 to 35 degrees and velocities of 5 to 10 m/s. Null and Shkarayev determined

that at high-speed flights the 3% camber wing would give the best performance because of its high lift to drag ratio however at the low-speed flights, the 6% and 9% cambers would produce better results.

Although the geometry of the wing plays a large role in the success of the MAV, Kunz and Kroo [5] determined that drag plays an even greater role. Kunz and Kroo conducted aerodynamic research on airfoils at low Reynolds numbers and concluded that the flow was dominated by viscous effects and thick boundary layers. Ultra-low Reynolds numbers produced very high drag coefficients and small changes in the Reynolds numbers lead to large changes in drag. Kunz and Kroo also acknowledged that geometric variations have a strong effect on airfoil performance as well.

Due to the strong similarities in flight regimes, researchers have begun to conduct research comparing MAV's to animals in nature such as small birds and insects. Tucker [6] conducted experiments with wing tip slots, similar to those of birds, at the end of low aspect ratio airfoils in hopes to reduce induced drag. A model of the design can be seen in Figure 5 above. Tucker discovered that the wing with feathered tips produced 12% less drag than that of a hypothetical wing with the same lift and span and concluded that the tip slots of birds reduce induced drag.

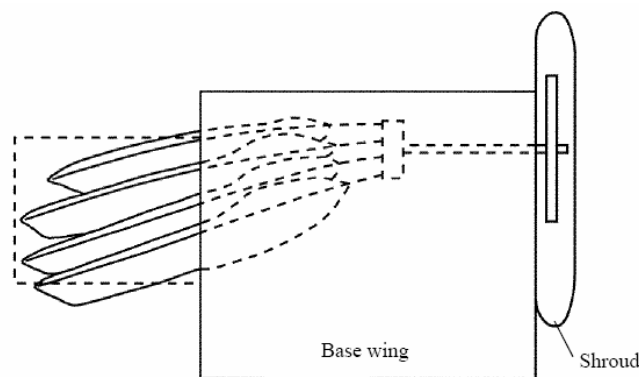


Figure 5: Design of Airfoil Containing Wing Tips [6]

Further research involving the flight regimes of birds was conducted by Drovetski [7]. Drovetski looked into the influence of trailing edge notches on the flight performance of four different species of galliformes and drew a significant number of conclusions from his research. After considering many factors including wing length-to-breadth ratio, notch size, wing loading, and the aspect ratio of the wing, Drovetski noticed an increase in lift to drag ratios when notches

were applied for all four species of birds. He also concluded that birds that spend a significant amount of their flight time in taking off with more vertical movement as opposed to long, fast, steady flight, have larger wing notches because greater lift to drag ratios significantly help in this process.

Ellington and Usherwood [8] also made comparisons between MAV wings and nature and examined the lift and drag characteristics of rotary and flapping wings by studying insect planforms such as the Hawkmoth wing. This also included investigation into trailing edge notches. Ellington and Usherwood identified only small differences in the coefficients of lift and drag versus angle of attack and no major differences in notched and unnotched planforms.

More research on trailing edge notches at low Reynolds numbers was conducted by Blanchard, DeFusco, and Donoghue [9]. It was hypothesized that these notches would reduce the amount of induced drag on the wing and contributes to increasing the lift to drag ratio when compared to un-notched wings. After placing notches on the wing naturally there is a decrease in lift however the hope was that the consequential decrease in total induced drag was greater, giving the aircraft an improved lift/drag (L/D) ratio.

In addition to determining if notched wings would increase the lift to drag ratio, the group also tried to determine the optimal size and locations of the notches. In order to isolate the optimal location they fixed the notch geometry and varied the location across the wing span. They discovered that, for their setup, notches placed at 60% of the half span produced the greatest L/D ratio. Results of their finding can be seen in Figure 6 below.

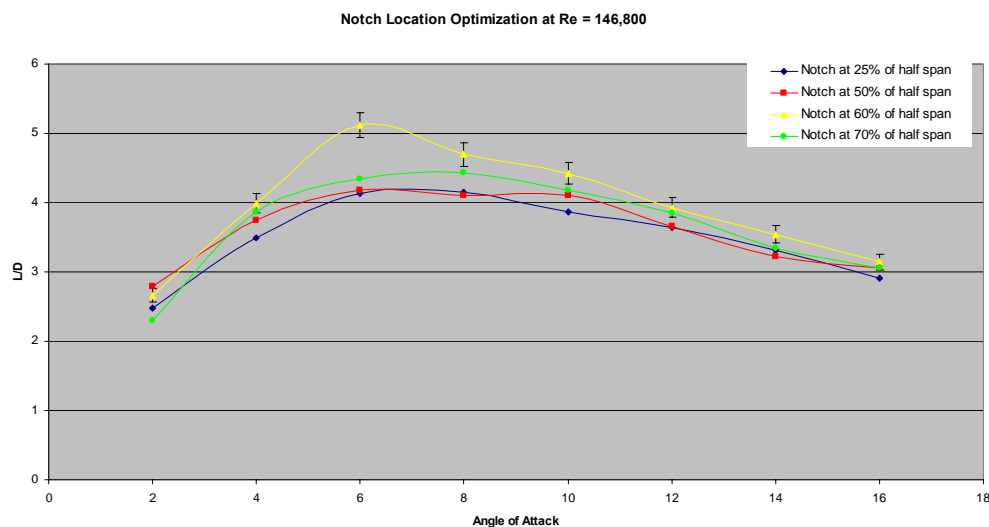


Figure 6: Comparison of Lift-to-Drag Ratios for Airfoils with Varying Notch Locations [9]

The geometry for the wing notches were equilateral triangles. Once the 60% half span optimal location was discovered, the sizes of these equilateral notches were adjusted to find the optimal size. They soon found that a pair of notches with 1” – long sides obtained the highest L/D ratio. These notches accounted for 1.76% of the total wing planform area. Figure 7 displays the group’s results below.

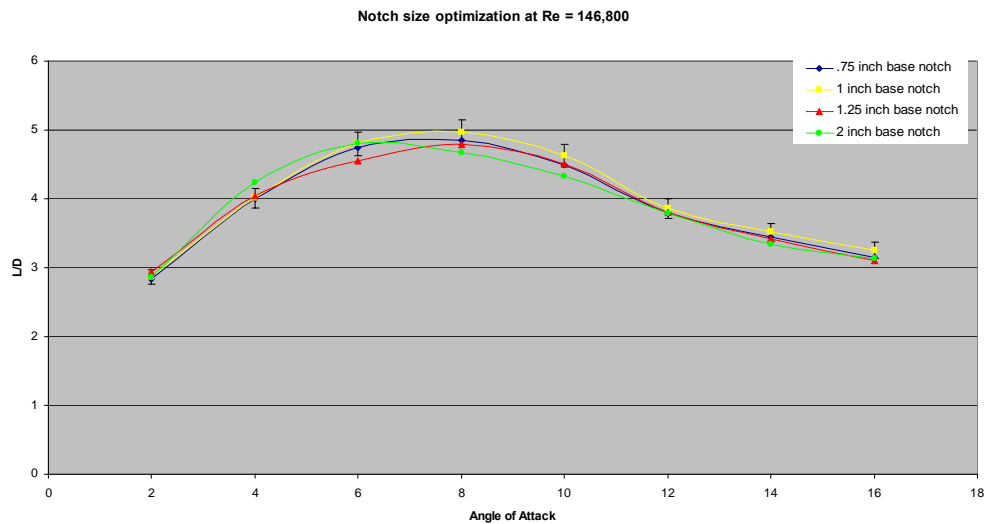


Figure 7: Comparison of Lift-to-Drag Ratios for Airfoils with Varying Notch Size [9]

Blanchard, Defusco, and Donoghue concluded that with the notch size and location optimized, the lift to drag ratio is greater with notches than without as seen in Figure 8 below. This seems to confirm the results obtained by Drovetski with trailing edge notches in bird wings but contradicts the results obtained by Ellington and Usherwood for flapping wings. Therefore further work is needed to confirm if notches are significantly improving the lift to drag ratio.

The main focus of this study will be to confirm Blanchard, Defusco, and Donoghue’s results. We will also apply notches to an already assembled MAV to see if trailing edge notches enhance endurance and range.

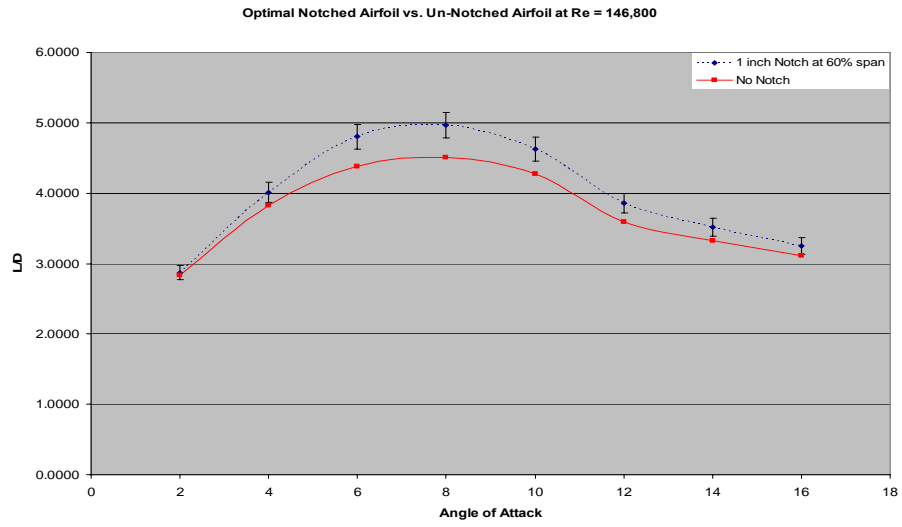


Figure 8: Optimal Notched Airfoil vs. Unnotched Airfoil [9]

1.3 Project Objectives

The objectives of this project are:

- To study the effects of trailing edge notches through wind tunnel testing of low aspect-ratio wing ($AR=1$) at Reynolds numbers ranging from 50,000 to 172,000 specifically:
 - To prove that trailing edge notches decrease total induced drag.
 - To prove that the reduction in drag is greater than the overall loss in lift, thus increasing lift to drag ratios.
- To compare the L/D data collected this year to the previous study conducted by Blanchard, DeFusco, and Donoghue [9].
- To conduct flight tests on an MAV to determine if trailing edge notches improve flight endurance and range.

In this project we sought to further demonstrate that trailing edge wing notches can improve MAV flight performance (low aspect ratio, low Reynolds number flight regime 50,000~172,000) by producing a greater L/D ratio. The previous year's WPI MQP group obtained some preliminary results about trailing edge notches, such that they are capable of increasing L/D ratios for a given wing profile. This was a valuable base for the overall study however the data had to be first validated before moving on to the next phase of the project.

In order to get started we had to rebuild the MAV force balance that was used the previous year. The exact same design for the balance was used with only one modification. The previous year experienced a problem known as cross-talk. If a lift is applied to the force balance, ideally there should be no drag. However due to moments in the force balance there was a measurable drag effect when a lift was applied. This is known as cross-talk. In the new force balance design this problem was addressed.

After calibration of the force balance, data collection was conducted in the same method that it was in the previous year. Once positive and consistent data was produced with a flat plate airfoil, notches were applied to an actual MAV and flight testing was completed to study the effects of notches on a cambered MAV aircraft.

Section 2: Methodology

2.1: Design of the Force Balance

In attempting to recreate the results produced by Blanchard, Defusco, and Donoghue [9], the same experimental equipment had to be used. However due to the unavailability of the previous force balance, we found it necessary to replicate their design and construct a new force balance. Blanchard, Defusco, and Donoghue's report was consulted during the construction and this section will discuss each aspect of the force balance. A detailed description of the construction of the force balance including dimensions and building methods are presented in Appendix A.

2.1.1: Base

The most important component to the force balance was the base. The base would be sitting directly on the scales to measure lift and also hold the stand and proximeter where horizontal movement would measure the drag. The base was constructed using T-Slot aluminum allowing for a very simple construction process free from welding or drilling into the metal. All construction involved screws, washers, and L-brackets to reduce motion in the base. Figures 9-12 below show the force balance from each of the four sides.



Figure 9: Base - Side A

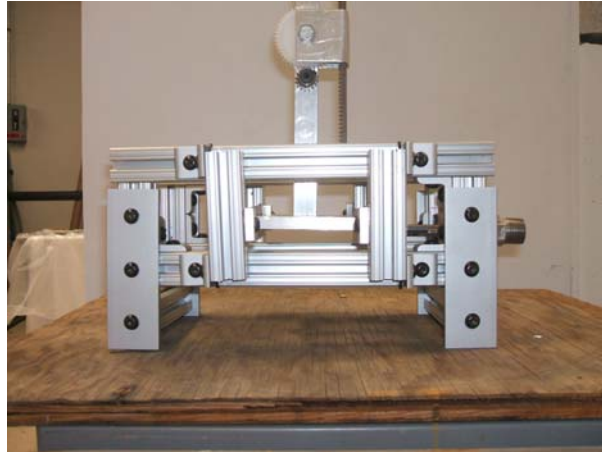


Figure 10: Base – Front

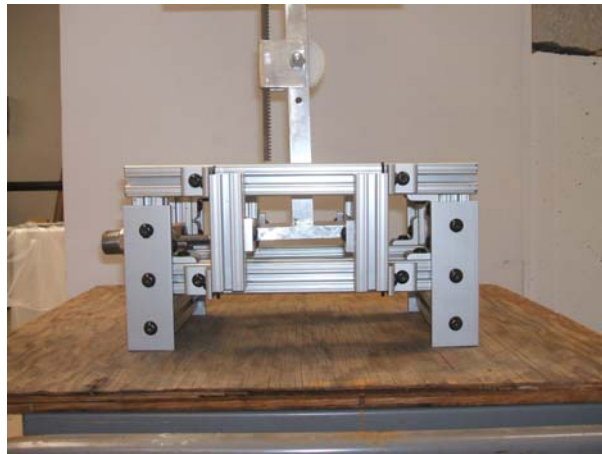


Figure 11: Base – Back

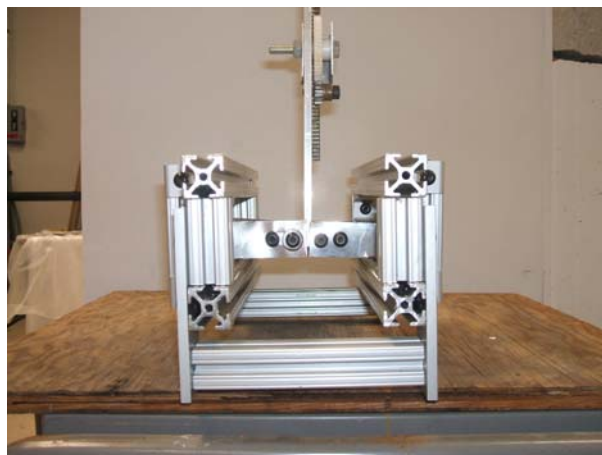


Figure 12: Base - Side B

Figure 9 shows the wood block which held the proximeter in place. Wood was chosen over metal for a few reasons. The first being that if the proximeter had to be replaced for any

reason by a different model than wood would allow for easy modifications. The precaution proved to be beneficial as the proximeter did have to be replaced midway through the project due to faulty electronics. The new proximeter was larger in diameter and it meant a new hole had to be drilled. Another reason wood was chosen was because it absorbed random vibrations much more effectively than metal, which seemed to amplify the vibrations. The precision of the drag measurements were extremely important and any vibration would disrupt the data. The final reason for wood was due to the modification made to the overall base design.

One of the goals set before the project began was to eliminate “cross-talk” from the force balance. One of the main reasons the design of the force balance was chosen was because if a pure lift was applied to it then theoretically the drag reading should still read as zero. However due to the length of the stand, a moment in the system was being created and therefore it distorted the drag readings. A crude visual example of what was happening can be seen in Figure 13. The location where the lift is applied is where the airfoil sits, the long vertical shaft is the stand and the square base at the bottom is the part that sits in the force balance base. When the lift was applied, the drag might read as an increase or decrease depending on where the proximeter was located. The modification on the base allowed the wood block and proximeter to move up and down vertically to find the point where there was zero moment and therefore a zero drag reading.

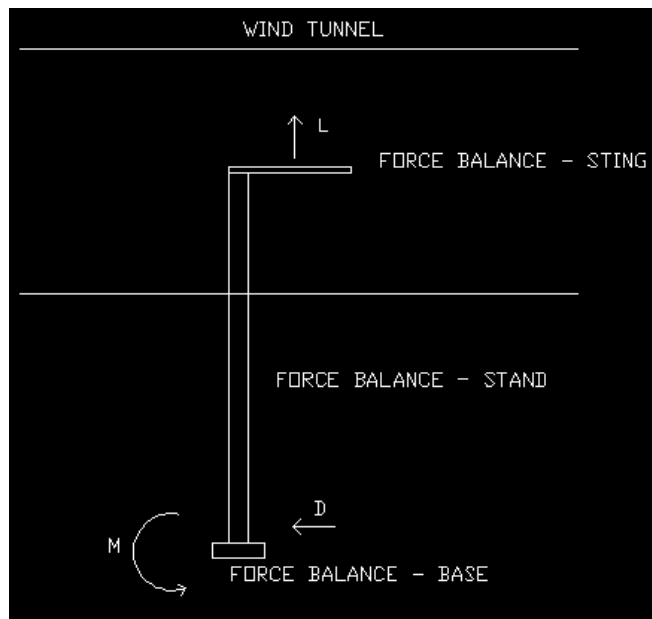


Figure 13: Lift/Drag/Moments Diagram

Both Figures 12 and 14 show how the steel shims are set up. Four thin, steel shims extend from the two sides of the force balance base and attach to the front and back of the stand base. The shims are thin enough to allow motion in the horizontal direction but still sturdy enough to keep the stand from sinking. On the side which meets with the proximeter is a thin piece of steel attached on top of the two shim pieces. This is necessary in order for the proximeter to measure a voltage difference when there is horizontal force applied to the stand.

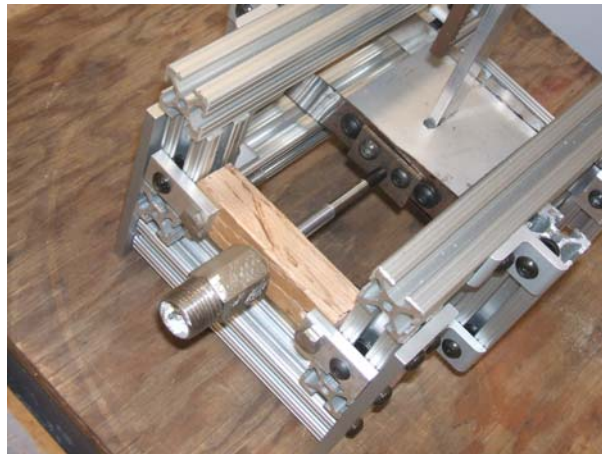


Figure 14: Base - Top

2.1.2: Stand and Sting

The other components to the force balance were the stand and sting. As described before, the stand sat directly in the force balance base and attached to the top of it was the sting which would hold the airfoil in place. Fortunately, the previous stand/sting components were still available from the previous MQP work and there was no need for a redesign or reconstruction. The most important aspect of the stand was that it allowed for the angle of attack to be easily changeable while it sat inside the wind tunnel. This was done by using a gear setup.

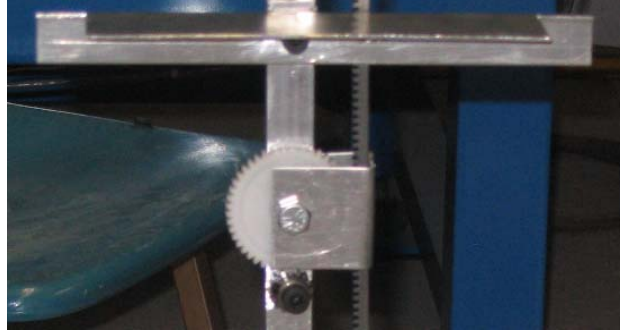


Figure 15: Stand - Gear Setup [9]

Figure 15 shows the gears used in adjusting the angle of attack. Working from the bottom up to describe how it works, the black gear is where an “L” shaped hex wrench can be used to create the turning motion. The distance between each tooth is very small which allows for fine adjustments in the angle of attack. The black gear is then attached to a larger plastic gear which in turn is attached to a skinny, vertical beam with gear teeth on one side. A clockwise turn with the hex wrench would increase the angle of attack and a counter-clockwise turn would cause a decrease. A thin aluminum plate is also attached to the vertical beam. This is where a digital angle scale can sit to read the angle of attack. At the top of the stand is where the sting is welded. The sting has the ability to pitch up or down when the angle of attack at the lower part of the stand is adjusted. This can be seen in Figure 16. Full CAD drawings of the stand and sting are presented in Appendix B.



Figure 16: Sting [9]

2.1.3: Final Design

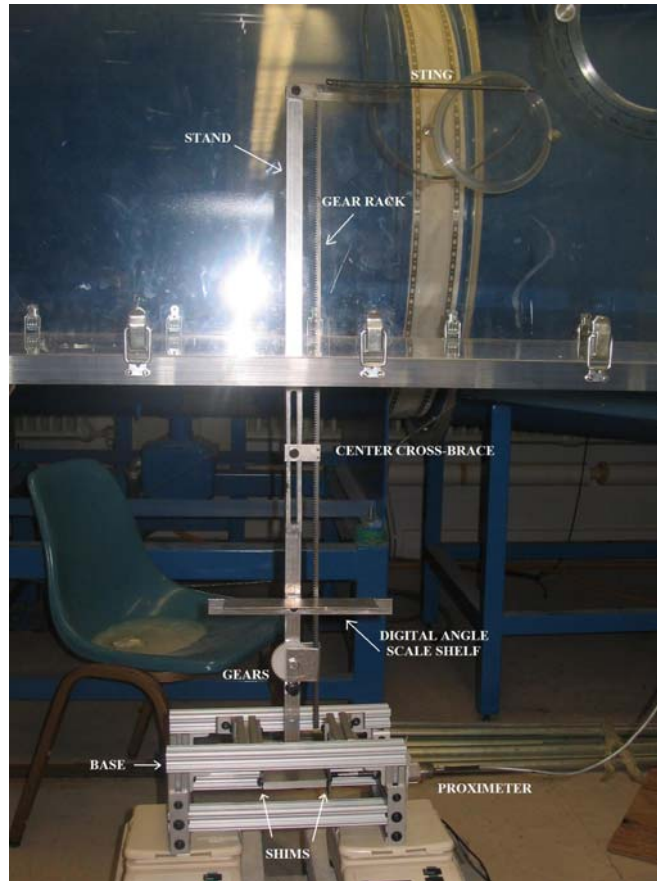


Figure 17: Force Balance [9]

Once the force balance is fully constructed and attached, Figure 17 shows the final setup for the force balance as it sits in the wind tunnel. The force balance passes through the bottom of the wind tunnel and allows for angle of attack adjustments during testing. The force balance rests on two digital scales to measure lift. Further discussion of the measurement of lift forces using the digital scales can be found later in the report.

2.2: Wind Tunnel Testing

The wind tunnel testing was conducted in order to collect lift and drag data on both notched and unnotched plates at a range of low speeds. However there were many steps that had to be taken to properly conduct the wind tunnel tests. This section will discuss each step and what the purpose was for doing it.

2.2.1: Setup

When setting up the force balance in the wind tunnel it was very important to set it up exactly the same way each time. Any small changes to the force balance location or setup would affect the results and therefore it was deemed necessary to collect full data sets all in one sitting. This eliminated the possibility of the force balance being disturbed when the group was not present in the lab.

Figure 17 shows how the force balance was setup in the wind tunnel. It was desired to have the airfoil sit in the middle of the wind tunnel. However this was not possible if the force balance had sat on the ground because the stand was not long enough. Therefore the force balance sat on two ACCULAB VI-2400 digital scales (at equal height) which sat on cinder blocks approximately 1.5 feet off the ground. In terms of the stream wise location of the airfoil, this was limited to one location due to the design of the wind tunnel. The location however, was adequate.

Though the positioning of the force balance on the scales should not matter (since no moments were being calculated, just forces), extra precaution was taken by standardizing the force balance placement. Marks were made on the scales to show where the left and right edges of the base should line up. This was also done to help produce repeatable lift scale readings between different data collection sessions for comparison if necessary. Arbitrary placement of the force balance would not allow for this since two scales were used to measure lift, and while an arbitrary placement should still have the same lift value, the readings on the left and right scales would not correspond to those found in previous data collection sessions. Being able to see the repeatability of values on each scale, aided in the understanding of why the “same” data collected on different days might not be equivalent due to a misplacement of the force balance.

Once the force balance was in place, the flat plate was secured to the sting through means of a screw and a cylindrical metal piece that was tightened (via a screw) to the sting. The placement of the plate was critical because if it was tilted ever so slightly to the left or right, the normal force generated on the plate during testing would not correspond directly to the lift force measured on the scales. Therefore much care was taken to ensure the proper placement, which also aided in the standardization of the testing procedure.

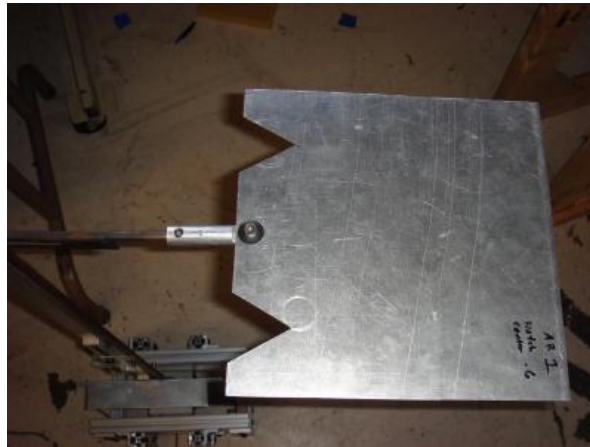


Figure 18: Flat-Plate Attached to Sting

Typically the proximeter would be placed in its housing before positioning the force balance since it was easier to tighten it into place on a table rather than under the wind tunnel. Early on in the project, the proximeter nuts were tightened by hand, but due to the extreme sensitivity of the new proximeter, it was found necessary to secure the proximeter more tightly into place by using wrenches rather than hands. The proximeter was positioned such that it had a beginning offset voltage due to being a certain distance away from the metal plate it interacted with. An offset voltage between 2.5 V and 4.5 V was chosen and will be discussed in the next section.

2.2.2: Measuring Forces

The two forces which were being measured in the wind tunnel were the lift and drag on the thin plate airfoil. To measure the lift, the force balance was placed on two simple digital scales that can be found in any chemistry or physics labs. They had an accuracy rating of +/- 0.1 gram (each). The choice to use two scales resulted from the facts that our force balance was too heavy to be supported solely by one scale, and secondly that if it was desired to go back to the data and calculate moment coefficients and centers of pressure, it would be possible to do so.

The first scale was placed at the proximeter end of the base and the second scale at the other end. Before turning the wind tunnel on, both scales were zeroed. Finally the tunnel was turned on to the desired speed and the scales were read. Naturally when the airfoil begins to feel a lift force, the front of the force balance base (the proximeter end) will begin to lift giving a negative value on the first scale and the back of the force balance base (the non-proximeter end) will feel a force and give a positive value. These two values were then added together to provide the total lift and magnitude on the airfoil. The scales can be seen in Figure 19 below.



Figure 19: Digital Scales

The drag reading involved the use of the proximeter. A proximeter measures a voltage difference proportional to the gap between the proximeter tip and the steel plate attached to the stand base. The proximeter was inserted through the block of wood on the force balance base and moved close enough to the steel plate so that it would provide a reading of 2.5 – 4.5 V. The range in volts in terms of distance is approximately 1/8 of an inch. The reason 2.5 – 4.5 V was used was due to experience gained while using the proximeter during drag calibrations. It was determined that this voltage range provided the most consistent results and offset voltages greater than 5.0 V typically started to appear to be less sensitive. Once the proximeter was set in the desired location it was tightened down, the signal was sent to an amplifier, and the amplifier was connected to a Hewlett Packard 3478A Multimeter which displayed the voltage to the nearest millivolt. Once the wind tunnel was turned on the drag on the airfoil would cause a horizontal motion increasing the gap between the proximeter and the steel plate and also increasing the voltage read by the multimeter. The difference between the initial voltage and

final voltage was found and then converted into grams using the previous drag calibration, henceforth providing a drag reading.

2.2.3: Drag Calibration

Since the proximeter simply measured changes in linear displacement as a voltage, it was necessary to convert these displacement/voltage readings into drag forces. A drag calibration process was needed that could compare known drag forces to changes in output voltage readings from the proximeter. After going through many iterations and ideas, the final decision was made to hang a fishing line from the tunnel ceiling downstream of the sting and connect the other end of the fishing line to the sting. By placing weights along this string at a very specific location, 45 degree angles could be made at each line-supporting location (the tunnel ceiling and the sting itself) ensuring that half of the weight hung would correspond to the amount of drag force being applied to the sting. This idea was derived from the previous year's MQP who used essentially the same setup with the fishing line placed at locations different from ours. There was some difficulty in repeating their setup and ensuring that the fishing line made 45 degree angles at both supports. Therefore using the knowledge that the weight would be equally supported from each support, it could be confirmed that 45° angles were being produced at both supports when the scale readings on the sting side measured half of the weight placed on the fishing line. This concept enabled us to very quickly and accurately perform drag calibrations.

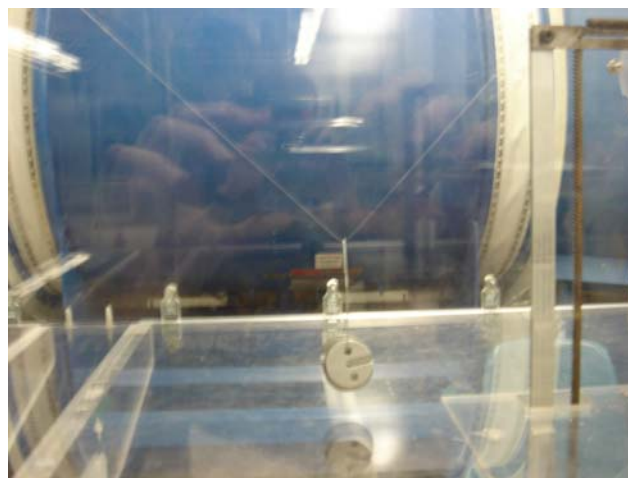


Figure 20: Drag Calibration Setup

Once the drag calibration fishing line was properly attached, the drag calibration began by hanging small weights on the fishing line. A 5-gram mass was initially used in order to ensure the fishing line was taut and in the proper location. After taking the baseline voltage, the weight on the string was increased in the following manner: 0, 10, 20, 30, 40, 50, 60, 80, 100, 120 grams and the output voltage was taken after each additional weight was added. This enabled us to plot the known drag force in grams vs. the voltage output by the proximeter (mV) and allowed us to perform a linear regression to derive the proximeter calibration to be used.

Table 1: Drag Calibration Results

Mass [g]	Drag [g]	[V]	[mV]
0	0	3.108	3108
10	5	3.129	3129
20	10	3.161	3161
30	15	3.19	3190
40	20	3.214	3214
50	25	3.24	3240
60	30	3.267	3267
80	40	3.319	3319
100	50	3.375	3375
120	60	3.422	3422

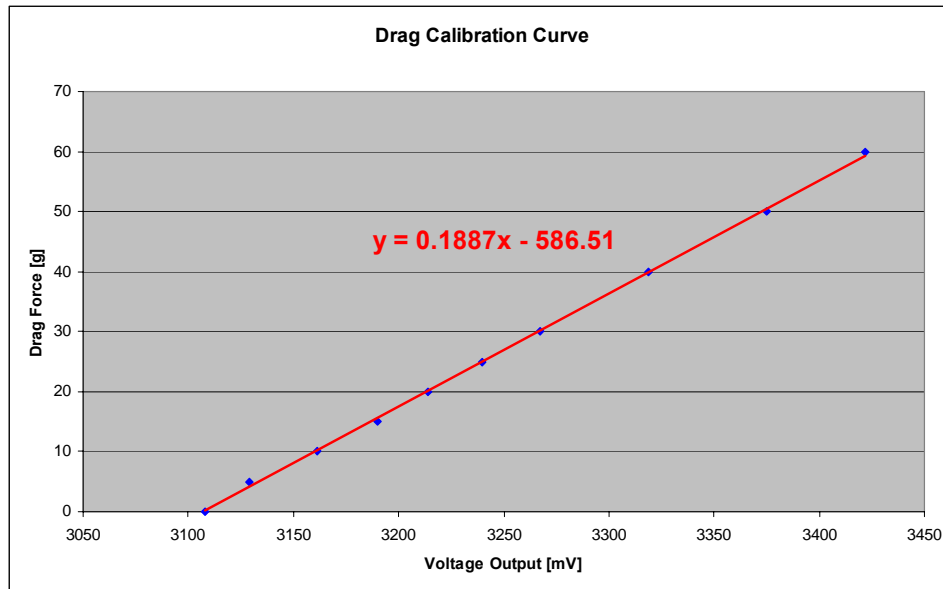


Figure 21: Drag Calibration Curve

Typically the drag calibration fell between .18 and .22 g/mV which meant that the force balance was able to read about 4.55 – 5.55 mV for every gram of drag measured. This was a very good resolution considering the range of deflection readings possible (on the order of volts as compared to millivolts). The multimeter was read to the nearest millivolt meaning that typically the error was +/- 0.5 mV or +/- 0.1 grams – a very small drag uncertainty which only has a significant impact at low angles of attack (2 to 4 degrees).

The drag calibration test was performed before each data collection session since some day-to-day variations were observed. This day-to-day variation was likely due to slight temperature variations, which would affect the spring coefficient of the thin steel shims, and more likely due to the movement of the force balance to and from the wind tunnel. The slightest banging against the side or pulling of the sting stand could have a significant impact on the calibration value, hence the need to run calibrations before each session. The drag calibration was also performed multiple times before each data collection session to ensure a repeatable value was present, as well as was checked at the end of a data collection session to ensure that the calibration value had not changed significantly.

2.2.4: Sting Drag Measurements

The drag force measured by the force balance included the drag on the flat plate in addition to the drag on the sting and portion of the sting stand which was present in the wind tunnel. Therefore the drag induced by the sting and stand had to be subtracted from the total drag measurement. This was done by placing the sting at zero degrees angle of attack, running drag measurements without the flat plate at a desired wind tunnel speed, and recording the drag value.

The question arose as to whether changing the angle of attack of the sting would have an effect on the force balance drag measurement, however no significant difference was observed. Therefore in the interest of saving time, only a drag measurement at zero degrees angle of attack was conducted. This test had to be performed before each data collection session since the voltage change would vary from day-to-day due to the drag calibration variation.

Further discussion arose later in the project about the effect of the sting drag and if simply subtracting it from the total drag value was sufficiently accounting for the total effects. Therefore it was decided to create a drag shield. The shield was created using steel shim and was simply bent in the shape of an airfoil so it could sit in the wind tunnel and cover the stand

without actually touching the stand. The overall goal of the drag shield was to almost completely eliminate the drag due to the sting stand assembly as well as drastically reduce the L/D values of the plots, thereby bringing them closer to ranges observed in other literature. The results of the effect of the drag shield will be discussed later in the report.



Figure 22: Force Balance Stand with Drag Shield

2.2.5: Data Collection

Due to the sensitivity of the force balance and the day to day variations in operation, it was found necessary to standardize the data collection procedure in the following manner:

1. Place force balance into wind tunnel in desired position on scales and at desired height in tunnel
2. Attach flat plate
3. Perform drag calibration (at least 3 times and take the average)
4. Remove flat plate
5. Perform sting drag measurement
6. Attach unnotched flat-plate
7. Run “solid plate” tests
 - a. Set desired angle of attack
 - b. Reset digital scales
 - c. Record reference voltage
 - d. Run wind tunnel at desired speed
 - e. Record readings on digital scales

- f. Record voltage
 - g. Turn off wind tunnel and check that the voltage returns to the reference voltage
 - h. If voltage reading is different from reference voltage, take new voltage as reference, re-run wind tunnel and update voltage readings -- Repeat until reference voltage matches voltage after wind tunnel is turned off
 - i. Repeat process for remaining angles of attack
8. Look for erroneous data points / double check data points for consistency
 9. Carefully replace unnotched plate with notched plate
 10. Run “notched plate” tests
 11. Look for erroneous data points / double check data points for consistency
 12. Check drag calibration
 13. Repeat Steps 6-12 for different speed or configuration

The data collection procedure is very straightforward however several small, but important details must be discussed. When measuring drag forces, as in Step 7 above, a reference voltage must be taken before running the wind tunnel for comparison. If the voltage does not return to this reference voltage when the wind tunnel is turned off, something in the force balance setup has changed (most likely the shims have not returned exactly to their original position). Therefore the drag measurement must be done iteratively until the voltages before running the tunnel and after shutting down the tunnel match. We found that we typically had to run the tunnel at least twice per angle of attack to ensure this was the case.

When reading the lift scales, some fluctuation is present due to the slight “wobbling” or vibrating of the force balance. In order to accurately read lift forces the scales must be read simultaneously. This was done by picking a value present on the left scale, waiting for it to appear on the right scale, and then immediately reading the corresponding value from the left scale. At high angles of attack and high wind tunnel speeds, this can be extremely difficult due to the quickly changing values on the scales. Taking a picture with a digital camera gave a quick snapshot of the scales and made it possible to get a reading. It should be noted that the “wobbling” did not affect the total lift value, it just shifted the weight back and forth between scales.



Figure 23: Scale Readings at Two Different Times

2.2.6: Induced Drag

The induced drag on an airfoil is the drag due to the lifting actions of the wing in the drag direction. In order to isolate this type of drag force, wingtip effects must be removed (or reduced as much as possible). Since the pressure above the flat plate is lower than the pressure below it, the air tends to flow from the bottom-to-the-top side at the wing tips, causing additional drag (not due to lift). Therefore if the airflow region about the wingtips can be “eliminated” this additional drag force can be eliminated. This was achieved through the use of wooden endplates placed in the wind tunnel as close to the flat plate as possible without actually touching the flat plate. The endplates spanned the entire height of the tunnel and were secured to the bottom surface with tape and to the top surface with foam wedges that greatly reduced the amount of swaying the endplates exhibited. The foam pieces were also necessary because the endplates used did not fully reach the ceiling of the wind tunnel for securing with tape. Reduction in swaying was extremely important when considering how close the endplates were located in order to eliminate wingtip effects (several millimeters). Any swaying at this close distance could have resulted in

the endplates contacting the airfoil thereby contaminating the experiment. By eliminating wingtip effects, the flow distribution across the airfoil became two dimensional in nature. After setting up the endplates in the wind tunnel, the data collection procedure was the same as that for the 3-D (no endplates) setup. The process of calculating the induced drag will be discussed further later in the report.

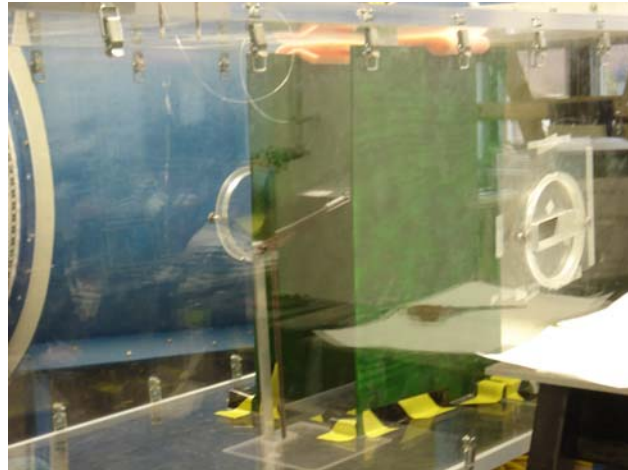


Figure 24: 2-D Wing Test Setup

2.2.7: Excel Data Sheet

To help keep track of the large amounts of data collected in each session, as well as the many parameters used to calculate desired values, an excel spreadsheet was created to standardize daily experiments. The files were typically named for the type of experiment being run (3-D, 2-D, other comparisons, etc.) as well as labeled with the date that the experiment was conducted. Typically each excel file would consist of the following sheets, which will be discussed in the following subsections:

1. Drag Calibration
2. Notchless Data / Notch Data
3. Last Year's Data
4. C_L vs. AOA
5. L/D vs. AOA
6. Current Year's Data vs. Last Year's Data

7. C_D vs. C_L^2

Drag Calibration

For standardization purposes the drag calibration for each data collection session used the same weights added in the same order. These weights were inserted into Column A. Column B was Column A divided by two because, as shown through a simple statics problem, only half of the weight placed on the string acted as a drag force on the force balance when the fishing line angles at each support were 45 degrees. These values, in grams, were the values that would be plotted to perform a linear regression. Column C was the voltage read off of the multimeter after the addition of each additional weight, and Column D is Column C * 1000 to convert volts to millivolts for plotting purposes. Once this data was collected, Column B (drag force in grams) was plotted vs. Column D (mV) and then a linear regression was performed in order to determine the calibration curve.

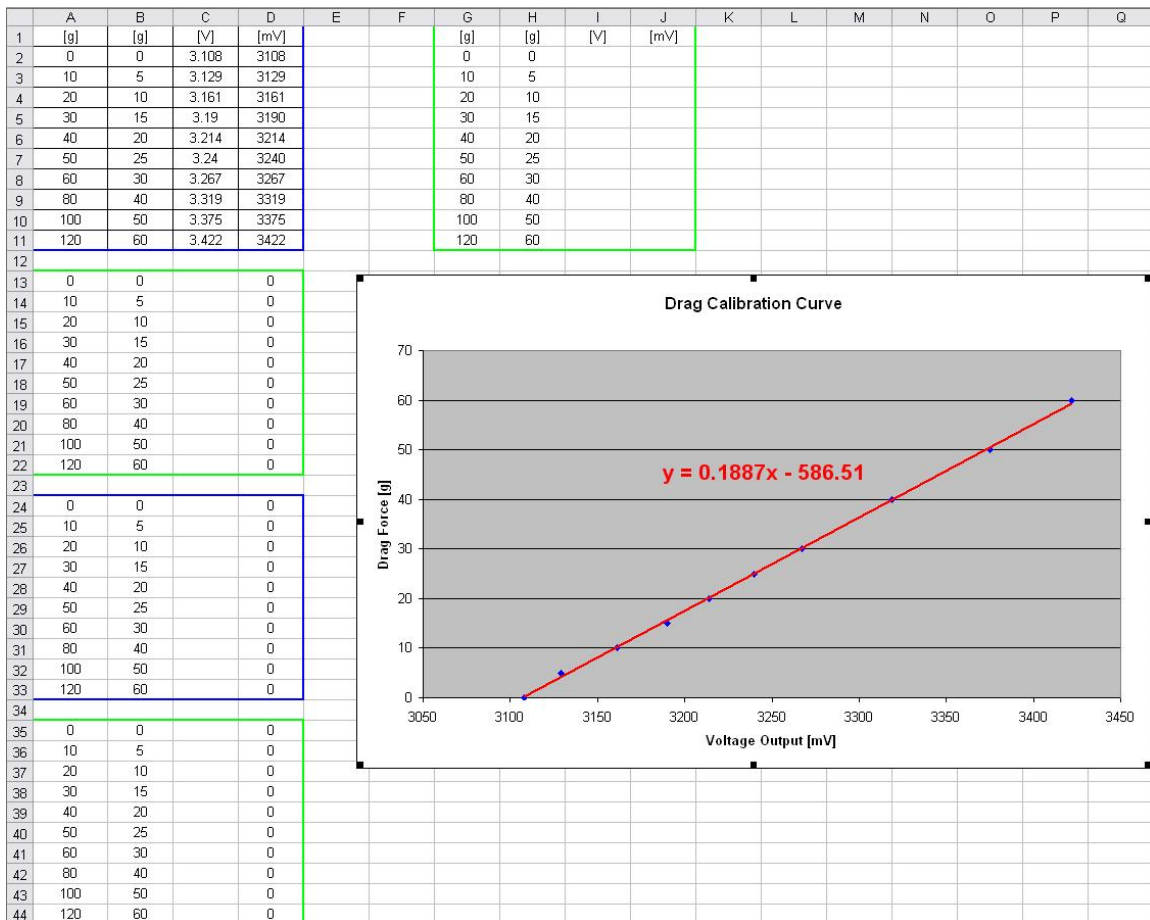


Figure 25: Drag Calibration Sheet

Notchless Data/ Notch Data Sheet

The notchless data / notch data sheets are the sheets containing all of the experimental data to be used for making plots and comparisons. Each sheet is the same with the exception of Column D, the planform area S. Since the notch wing configuration has less wing area, its value is 1.76% lower than the notchless planform area.

Column A, labeled **V [Hz]** is the wind tunnel setting in hertz. The wind tunnel operated as a function of its fan speed in hertz and this was converted to a more useful value **[m/s]** in **Column B**.

Column C, labeled **q_{inf}** is the dynamic pressure calculated in order to make later calculations in the spreadsheet simpler.

Column D, labeled **S** is the planform area of the wings tested, and as mentioned previously the values differ slightly for the notch and notchless configurations.

Column E, labeled, **Re** is the Reynolds number calculated for ease of reference later on for labeling plots and ensuring that we stayed within our desired Reynolds number limits.

Columns F and G are the **angles of attack** in degrees and radians respectively.

Columns H and I, labeled **S1 and S2** are the cells where the readings from the left and right scales (respectively) were entered for a given angle of attack.

Column J, labeled **Lift [g]** is the absolute value of (S1 + S2) and represents the lift force measured at a given angle of attack in grams. Column K is a conversion from grams to Newtons.

Column L, labeled **C_L** is the lift coefficient calculated from the acquired data and

Column M, labeled **C_L²** is the lift coefficient squared for use in C_D vs. C_L² plots.

Columns N and O are the initial (**V_i**) and final (**V_f**) voltage readings taken before running the wind tunnel and during wind tunnel operation respectively. **Column P** is Column O – Column N and represents the **difference in voltage readings (DV)** for calculation of a drag force.

Since the drag of the force balance assembly itself must be calculated for different speeds it is calculated and input into **Column Q** labeled **Sting DV**.

The Total DV is then **DV – Sting DV** and can be found in **Column R**. **Column S** is **Column R * 1000** for conversion to millivolts, and **Column T** is the **drag calibration [g/mV] * Column S [mV]** to yield the drag force on the flat plate in grams. This is converted to Newtons in **Column U (Drag [N])**.

Column V, labeled C_d is the drag coefficient calculated from the drag force, q_{inf} , and S .

Column W, labeled L/D , is the lift over drag ratio for a given angle of attack and Reynolds number. The values were calculated directly from the experimentally measured forces (in grams) rather than the lift and drag coefficients to reduce the chance of any data calculation errors.

Columns X-AA, if used, are calculations performed to acquire **errors bars for L/D** plots.

A	B	C	D	E	F	G	H	I	J	K	L	M	N	O	P	Q	R	S	T	U	V	W	X	Y	Z	AA		
YIBJ	YIAD	YIUM	SLM2I	BE	ADJLEAD	ADJLEAD	SI	S2	LITLJ	LITLJ	C.L	C.L2	YIYJ	YIYJ	DYIY	StngDY	TotalDY	TotalDY	TotalDY	EDJLEAD	DJLEAD	C.J	LJD	LJDHigh	Difference	LJDLow	Difference	
1	5	346	0.0387	48E204	2	348E-02			0	0.000	0.0000	0.0000			0	0.009	-0.009	-9	-1881	-0.077275	-0.0604262	0.000						
2	5	346	0.0387	48E204	4	638E-02			0	0.000	0.0000	0.0000			0	0.009	-0.009	-9	-1881	-0.077275	-0.0604262	0.000						
3	5	346	0.0387	48E204	6	109E-01			0	0.000	0.0000	0.0000			0	0.009	-0.009	-9	-1881	-0.077275	-0.0604262	0.000						
4	5	346	0.0387	48E204	8	140E-01			0	0.000	0.0000	0.0000			0	0.009	-0.009	-9	-1881	-0.077275	-0.0604262	0.000						
5	5	346	0.0387	48E204	10	179E-01			0	0.000	0.0000	0.0000			0	0.009	-0.009	-9	-1881	-0.077275	-0.0604262	0.000						
6	5	346	0.0387	48E204	12	208E-01			0	0.000	0.0000	0.0000			0	0.009	-0.009	-9	-1881	-0.077275	-0.0604262	0.000						
7	5	346	0.0387	48E204	14	244E-01			0	0.000	0.0000	0.0000			0	0.009	-0.009	-9	-1881	-0.077275	-0.0604262	0.000						
8	5	346	0.0387	48E204	16	278E-01			0	0.000	0.0000	0.0000			0	0.009	-0.009	-9	-1881	-0.077275	-0.0604262	0.000						
9	5	346	0.0387	48E204	18	278E-01			0	0.000	0.0000	0.0000			0	0.009	-0.009	-9	-1881	-0.077275	-0.0604262	0.000						
10	5	346	0.0387	48E204	2	348E-02			0	0.000	0.0000	0.0000			0	0.022	-0.022	-22	-4498	-0.0432962	-0.059792	0.000						
11	5	346	0.0387	48E204	4	638E-02			0	0.000	0.0000	0.0000			0	0.022	-0.022	-22	-4498	-0.0432962	-0.059792	0.000						
12	5	346	0.0387	48E204	6	109E-01			0	0.000	0.0000	0.0000			0	0.022	-0.022	-22	-4498	-0.0432962	-0.059792	0.000						
13	5	346	0.0387	48E204	8	140E-01			0	0.000	0.0000	0.0000			0	0.022	-0.022	-22	-4498	-0.0432962	-0.059792	0.000						
14	5	346	0.0387	48E204	10	179E-01			0	0.000	0.0000	0.0000			0	0.022	-0.022	-22	-4498	-0.0432962	-0.059792	0.000						
15	5	346	0.0387	48E204	12	208E-01			0	0.000	0.0000	0.0000			0	0.022	-0.022	-22	-4498	-0.0432962	-0.059792	0.000						
16	5	346	0.0387	48E204	14	244E-01			0	0.000	0.0000	0.0000			0	0.022	-0.022	-22	-4498	-0.0432962	-0.059792	0.000						
17	5	346	0.0387	48E204	16	278E-01			0	0.000	0.0000	0.0000			0	0.022	-0.022	-22	-4498	-0.0432962	-0.059792	0.000						
18	5	346	0.0387	48E204	2	348E-02			0	0.000	0.0000	0.0000			0	0.022	-0.022	-22	-4498	-0.0432962	-0.059792	0.000						
19	5	346	0.0387	48E204	4	638E-02			0	0.000	0.0000	0.0000			0	0.022	-0.022	-22	-4498	-0.0432962	-0.059792	0.000						
20	5	346	0.0387	48E204	6	109E-01			0	0.000	0.0000	0.0000			0	0.022	-0.022	-22	-4498	-0.0432962	-0.059792	0.000						
21	5	346	0.0387	48E204	8	140E-01			0	0.000	0.0000	0.0000			0	0.022	-0.022	-22	-4498	-0.0432962	-0.059792	0.000						
22	5	346	0.0387	48E204	10	179E-01			0	0.000	0.0000	0.0000			0	0.022	-0.022	-22	-4498	-0.0432962	-0.059792	0.000						
23	5	346	0.0387	48E204	12	208E-01			0	0.000	0.0000	0.0000			0	0.022	-0.022	-22	-4498	-0.0432962	-0.059792	0.000						
24	5	346	0.0387	48E204	14	244E-01			0	0.000	0.0000	0.0000			0	0.022	-0.022	-22	-4498	-0.0432962	-0.059792	0.000						
25	5	346	0.0387	48E204	16	278E-01			0	0.000	0.0000	0.0000			0	0.022	-0.022	-22	-4498	-0.0432962	-0.059792	0.000						
26	5	346	0.0387	48E204	2	348E-02			0	0.000	0.0000	0.0000			0	0.022	-0.022	-22	-4498	-0.0432962	-0.059792	0.000						
27	5	346	0.0387	48E204	4	638E-02			0	0.000	0.0000	0.0000			0	0.022	-0.022	-22	-4498	-0.0432962	-0.059792	0.000						
28	5	346	0.0387	48E204	6	109E-01			0	0.000	0.0000	0.0000			0	0.022	-0.022	-22	-4498	-0.0432962	-0.059792	0.000						
29	5	346	0.0387	48E204	8	140E-01			0	0.000	0.0000	0.0000			0	0.022	-0.022	-22	-4498	-0.0432962	-0.059792	0.000						
30	5	346	0.0387	48E204	10	179E-01			0	0.000	0.0000	0.0000			0	0.022	-0.022	-22	-4498	-0.0432962	-0.059792	0.000						
31	5	346	0.0387	48E204	12	208E-01			0	0.000	0.0000	0.0000			0	0.022	-0.022	-22	-4498	-0.0432962	-0.059792	0.000						
32	5	346	0.0387	48E204	14	244E-01			0	0.000	0.0000	0.0000			0	0.022	-0.022	-22	-4498	-0.0432962	-0.059792	0.000						
33	5	346	0.0387	48E204	16	278E-01			0	0.000	0.0000	0.0000			0	0.022	-0.022	-22	-4498	-0.0432962	-0.059792	0.000						

Figure 26: Notched/Unnotched Data Sheet

Previous Year's Data

The data from the previous MQP group (their best data set for each Reynolds number) was included as its own sheet for comparison purposes. Having their data embedded into each of the excel files also allowed for their data to be plotted along side the data that was collected this year, as will be discussed in the results section, to see whether or not we derived similar conclusions.

C_L vs. AOA, L/D vs. AOA, C_D vs. C_L^2 Plots

These plots are displayed on individual sheets in each excel file and display the pertinent data for comparisons between this year's data and last year's data as well as notched performance vs. no-notch performance. These plots will be discussed in further detail in the results section.

2.2.8: Error Bars

Since the results of the L/D study were very similar, it became necessary for the amount of experimental error to be quantified. The two possible areas for error existed in the measurement of the two forces: lift and drag. Since two digital scales were used for the measurement of lift, and each scale could be read to +/- 0.1 grams, the total lift error was determined to be +/- 0.2 grams.

The drag error was determined first by agreeing upon the number of decimal places that could be accurately read on the multimeter voltage output. The voltage error agreed upon was +/- .5 mV. Since the drag force depends on the calibration used, this error voltage had to be multiplied by the calibration in order to determine the drag error in grams.

The error bars were utilized on the 3-D L/D plot to aid in the determination of whether or not the notched or un-notched wing possessed more favorable performance characteristics. Since the L/D plot incorporates data from the lift and drag forces, the high error bar and low error bars represented two different scenarios. The high error bar represented the case when the lift force was at its upper error limit and the drag force was at its lower error limit, while the low error bar represented when the lift force was at its lower error limit and the drag force was at its upper error limit. The following equations make this clearer:

Upper L/D Error Bar:

$$\frac{L}{D} = \frac{L + 0.2}{D - (0.5) * k} \quad (1)$$

Lower L/D Error Bar:

$$\frac{L}{D} = \frac{L - 0.2}{D + (0.5) * k} \quad (2)$$

Where k represents the drag calibration in [g / mV]

One important note to make is that the error decreases as the forces on the wings increase. This can be seen from the L/D plot where at the lower angles of attack the errors are larger than at higher angles of attack.

2.3: Micro-Air Vehicle Testing

Another aim of this project is to investigate whether trailing edge notches affect the endurance, range, or flight performance of an actual MAV in flight. Tethered flight (or lasso) tests were conducted where the MAV flies in a circle around a pivot held by a team member. Our MAV flight tests examine how changing the lift to drag ratio with trailing edge notched affects the endurance and range of MAV's. Before beginning testing a new MAV had to be constructed as well as a test rig, and the parameters of the experiment had to be defined. The following sections describe the new aircraft, the methodology of the flight tests, the results, and conclusions drawn from them.

2.3.1 MAV Design

Originally the aircraft chosen as the test vehicle for the experiments was an MAV built in 2001 by a previous MQP team here at WPI [12]. The aircraft had been successfully flown many times and was known to possess stable flying characteristics well suited for our needs. However, since the 2001 MAV's last actual flight, modifications were made to it that rendered it un-flyable. It was decided to build a new MAV using the previous aircraft as a legacy airplane.



Figure 27: 2001 MAV

Having identified several of the deficiencies of the older MAV, the new MAV has several major improvements. Most drastic is the elimination of the rearward top-side fuselage. This serves to both decrease weight and increase the overall lifting surface of the MAV. Unlike the legacy aircraft, the airfoil of the new MAV is now maintained along the entire wingspan

increasing the wing planform area. A set of precisely cut jigs and a foam cutter was used to accurately shape the delicate Selig 5020 airfoil of the wing sections. This resulted in more accurate and more uniformly cut wings than for the previous MAV. The elimination of the Kevlar and heat shrink covering led to a significant weight savings. The 2007 MAV weighs a mere 172 grams compared with the 2001 aircraft at 293 grams, a weight savings of approximately 41%. We believe the elimination of the covering also yielded a significant decrease in drag. Additionally a lighter packaging tape was used over fiberglass tape as the hinging mechanism for the elevons.

A beneficial advancement in micro-aviation electronics which was employed in the new MAV was a new set of batteries. The old Nickel Cadmium (NiCad) batteries were eliminated in favor of Lithium Polymer (LiPoly) batteries. This drastically increased the power available from 600 mAh at 7.2 volts to 910 mAh at 11.1 volts. It also led to a weight savings of approximately one ounce as the LiPoly batteries weigh about 3 oz. to the NiCad 4 oz. The original receiver, a Hitec micro 555, was also replaced with a smaller and much lighter GWS 4 channel micro-light receiver. This not only decreased overall weight but also took up less space in the small central fuselage and made statically balancing the aircraft easier.

Other major improvements were made to the propulsion system. A new HiMaxx HA-4200 brushless electric motor replaced the older, larger brushed Graupner Speed 400. The HiMaxx motor is lighter, physically smaller, and much more efficient producing more thrust at lower throttle settings than the old 400. Additionally, the heavy folding prop and associated spinner was replaced with a fixed propeller and hub. This lighter setup has three main advantages. First it is much lighter and decreases overall aircraft weight. Second it allows the motor to achieve higher rpm's by decreasing the load on the drive shaft. Finally it makes balancing the airplane much easier due to the decrease in weight at the extreme front end of the aircraft.

The final major improvement to the MAV was the introduction of a test hard point for the attachment of the "lasso" tether to be used for tethered flight tests. The hard point is a hollow hard plastic tube which runs through one wing into the fuselage. Some monofilament fishing line is run through the tube and secured inside the fuselage via a knot. This hard point ensures that the stresses induced by the lasso are compressive rather than tensile due to the weak tensile strength of the foam airplane. Initially only one of the new aircraft was fully assembled; however

three full airframes and wing sets were produced allowing for the assembly of two additional airplanes in the event of a crash. This proved highly useful during testing.



Figure 28: Redesigned MAV - 2007

2.3.2 MAV Testing

The tethered flight tests were conducted by using a “lasso” system. This involved attaching a piece of string to the MAV which would be flown in a circle of set radius at a prescribed throttle setting until the batteries no longer possessed the energy to power the motor. This was done with both no notches and notches and the data was recorded to see if there was any effect on flight endurance and range.

To illustrate the effect of L/D on endurance and range we consider the Breguet equations [11]. For endurance:

$$E = \frac{L/D}{C} * \ln \frac{W_i - 1}{W_i} \quad (3)$$

Where E is endurance, C is specific fuel (energy for electric aircraft) consumption and the natural log term the weight fraction. For electric aircraft the weight fraction ($\ln \frac{W_i - 1}{W_i}$) must be re-interpreted. However because no significant weight changes are made between our tests this factor can be eliminated when comparing notched to un-notched endurance. The same is true for the specific energy consumption, C ; because each test is run at the same throttle setting which yields the same C .

Therefore,

$$\frac{E_{notched}}{E_{unnotched}} = \frac{\frac{(L/D)_{notched}}{C} \ln \frac{Wi-1}{Wi}}{\frac{(L/D)_{unnotched}}{C} * \ln \frac{Wi-1}{Wi}} = \frac{(L/D)_{notched}}{(L/D)_{unnotched}} \quad (4)$$

From this it becomes apparent that the lift to drag ratio is the sole factor in determining the endurance for this specific setup. Thus a 10% increase in notched L/D should lead to a 10% increase in endurance. Should the notched configuration lead to a decrease in L/D, it would result in a decrease in endurance as well. The range equation is similar:

$$R = \frac{V}{C} * \frac{L}{D} * \ln \frac{Wi-1}{Wi} \quad (5)$$

This leads to:

$$\frac{R_{notched}}{R_{unnotched}} = \frac{(V * \frac{L}{D})_{notched}}{(V * \frac{L}{D})_{unnotched}} \quad (6)$$

Here the weight fraction and specific fuel consumption terms are again eliminated and even though the throttle settings remain constant the velocity will not. Because there is an anticipated decrease in drag for the notched configuration (yielding an increased L/D) it was also anticipated that the notched aircraft would fly at a higher velocity for the same throttle setting. Thus the two velocities should differ but this does not present a difficulty. The increase in L/D would still result in an increase in range however it will now be augmented by the amount of increase in the velocity. A 10% increase in L/D that results in a 5% increase in velocity would yield 15.5% increase in range. Even if there is no appreciable difference in velocity, a change in L/D would still result in a change in the range.

The tests were completed indoors to control as many atmospheric variables as possible (wind speed, gusts, ambient temperature, etc.). The sole variable in each flight test was the configuration of the trailing edge of the wing. Before tests began, two identical triangular notches were cut into the elevons at 60% the half span of the wing. The area of both notches represented 1.76% the total wing planform area. This corresponded to the optimum performing notched airfoil as identified by Blanchard, Defusco, and Donoghue. To compare the notched

configuration to the un-notched, packaging tape was applied over the two notches to create “solid” elevons for the un-notched planform.

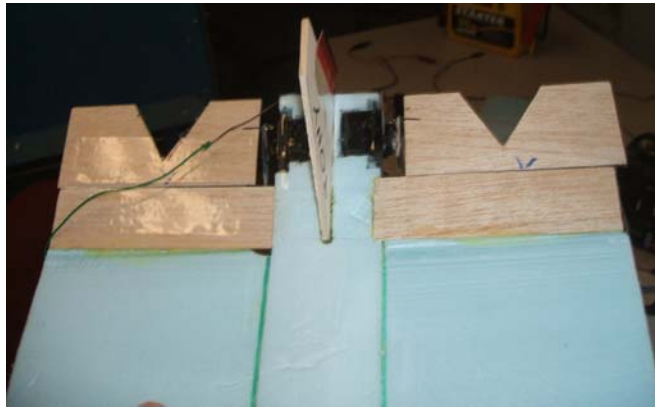


Figure 29: Notches Cut into Elevons

Several different styles of lasso testing were attempted and after two accidents and the total loss of one aircraft the following system was settled on as the most stable. One team member held the lasso at the center of the circle and slowly swung the aircraft around to “launch” it. As the airplane glided around the circle, the lasso holder allowed the string to slip out until it reached a set radius. We found it critical that the radius be large enough such that the aircraft would not travel too fast around the circle. If the radius is too short than this the aircraft had a tendency to become unstable in flight and fly in a vertical path as opposed to horizontal. This becomes very dangerous quickly as the aircraft approaches a “polar” orbit and risks striking the person or object holding the string. A second team member holds the controls and once the desired radius is achieved, the throttle is advanced to half. The team member holding the string would then stop swinging with the aircraft and stand still simply holding the line as a fixed pivot point. The aircraft would be allowed about 30 seconds to establish steady level flight before time would be officially started. The airplane was then to fly in the circle until the motor cut out and the flight time was to establish the duration of the flight. Filming each test allows the team to count the number of revolutions the aircraft made during the flight. Knowing the time of flight, the radius of the circle, and the number of revolutions we can then calculate endurance, range and velocity. Given these parameters our team then compared the performance of the notched configuration to the un-notched to establish if either yielded any appreciable advantage.

Due to problems of instability during flight tests, we were unable to fly the MAV until battery cut out. While stable flight was achieved for up to 5 minutes, any disturbance to the lasso

line caused the aircraft to become unstable. As team member's arms tired holding the lasso line, they were required to switch hands or switch out places with another team. This induced a disturbance in the line due to the change in elevation of the center point. When the MAV's flight became unstable the throttle had to be reduced to slow the aircraft down and control inputs were required to return it to stable flight. Once stability was regained the throttle was advanced again and the test resumed. This occurred an average of three to four times per flight. Because of the intermittent throttle changes and due to the required use of control inputs (which draw power from the battery), we could not assume that the specific energy consumption would be the same for all tests. Even if we had been able to fly the aircraft until battery cut out we would not have been able to use that time as the endurance due to the differences in energy consumption rates. However, we were able to assemble some data from our flights with a new methodology. The theory behind utilizing a notched airfoil assumes that an increase in L/D can be obtained by reducing a local lift peak and thereby also reducing the induced drag. This would in turn reduce the total drag on the aircraft. Thus if the total drag were reduced the aircraft should be able to achieve higher velocities for the same throttle settings. Since all of our tests involved flying our MAV at a set throttle setting, if we decided to compare any difference in velocity between the notched and unnotched test for a set time during which the aircraft was stable. If there was a significant change in total drag a different velocity should be seen.

Section 3: Results and Analysis

3.1: 3-D Test Results

3.1.1: C_L vs. α

According to Thin Airfoil Theory, a linear relationship exists between the lift coefficient C_L and the angle of attack α . The theory also states that the slope of the linear relationship is 2π such that the following equation represents the relationship between C_L and α :

$$C_L = 2\pi\alpha + C_{L_0} \tag{7}$$

Where α is in radians or:

$$C_L = 0.1097\alpha + C_{L_0} \tag{8}$$

Where α is in degrees. This relationship is illustrated by the following plots:

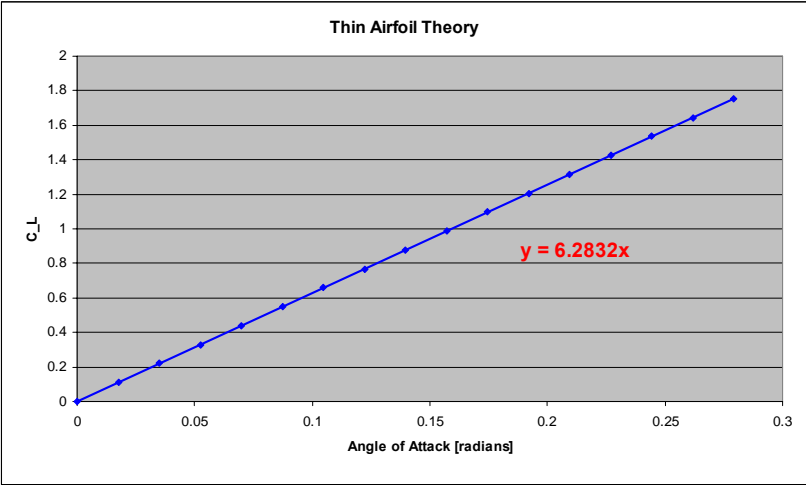


Figure 30: 3-D Coefficient of Lift vs. AOA (radians)

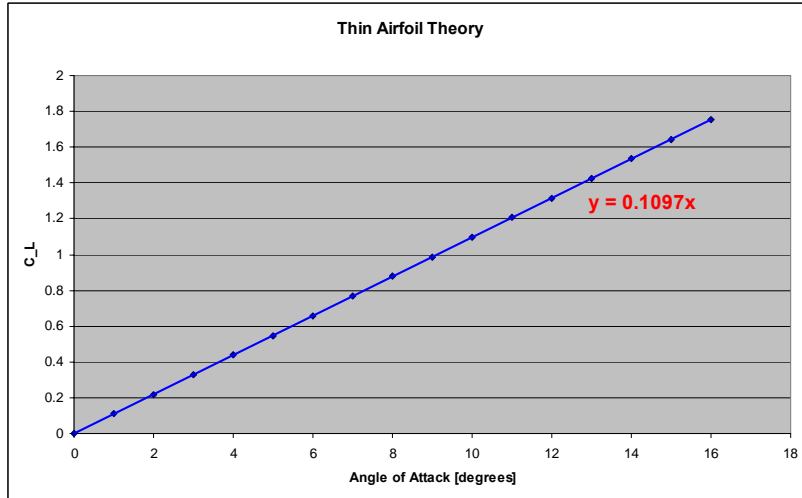


Figure 31: 3-D Coefficient of Lift vs. AOA (degrees)

Thin Airfoil Theory is not a true representation of a wing’s performance since it assumes the wingspan to be infinite (no wing tip effects). However it does provide us with an important concept that there is a linear relationship between a wing’s lift coefficient and angle of attack. Therefore throughout our experiments we expected to find a linear relationship between our C_L values and their corresponding angles of attack. But since our wings in the 3-D study were not of infinite span we expected to find that the slope of our C_L vs. α plot to be linear yet less than the slope suggested by the idealized Thin Airfoil Theory. Our results confirmed these trends:

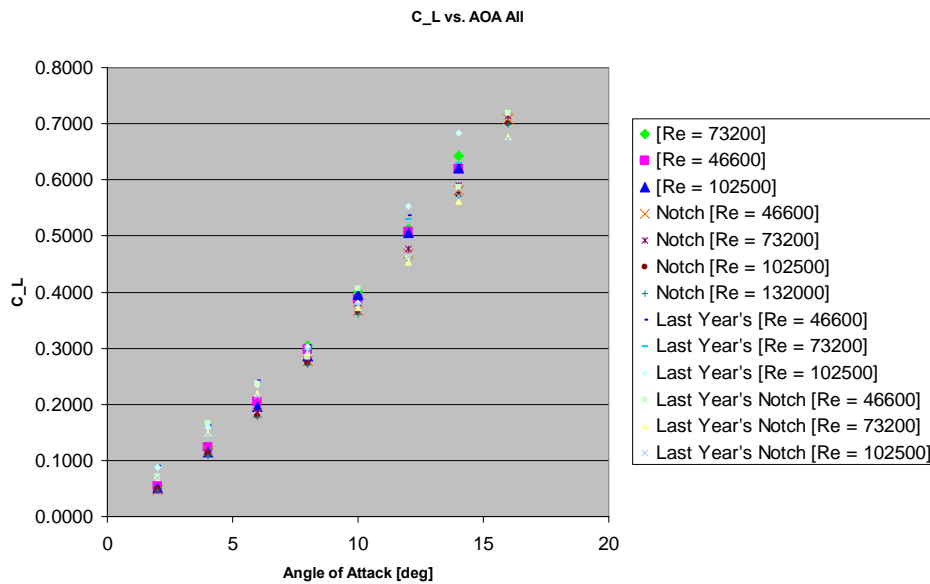


Figure 32: 3-D Coefficient of Lift vs. Angle of Attack Comparison

Figure 30 shows the expected linear relationship between the coefficient of lift and the angle of attack. We also observed that the measured lift coefficients agree well with data from Blanchard, Defusco, and Donoghue [9]. Looking more closely at one Reynolds number demonstrates how it compares to Lifting Line Theory:

$$C_L = \frac{2\pi(AR)}{AR + 2}(\alpha) \quad (9)$$

$$C_L = \frac{2\pi}{3}(\alpha) \quad (10)$$

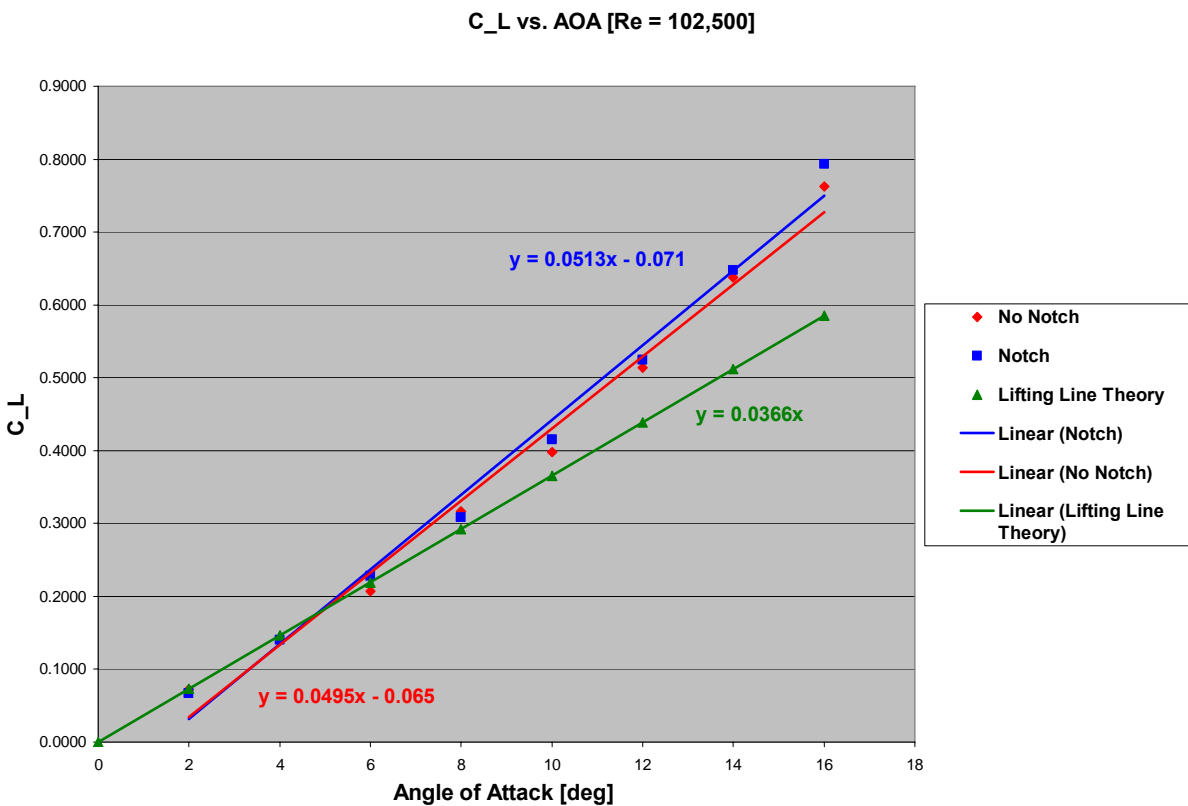


Figure 33: 3-D Coefficient of Lift vs. Angle of Attack compared to Lifting Line Theory

Lifting Line Theory represents Thin Airfoil Theory corrected for non-infinite wings. The next question to answer was whether or not there was any significant difference between the slopes of the no-notch and notched wings. The following plots illustrate the results:

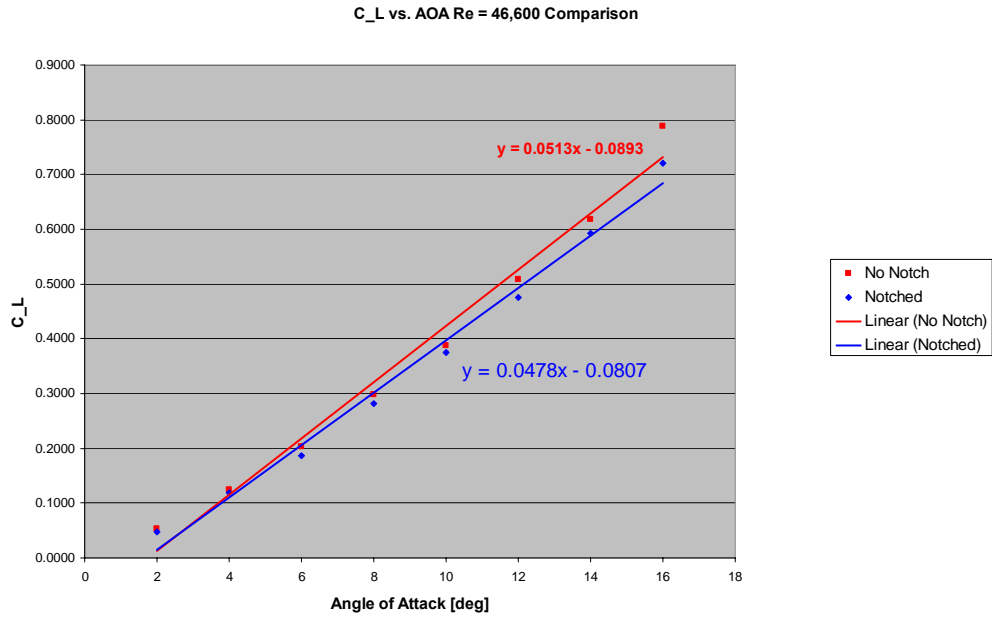


Figure 34: 3-D Coefficient of Lift vs. Angle of Attack for Notched/Unnotched–Re=46,600

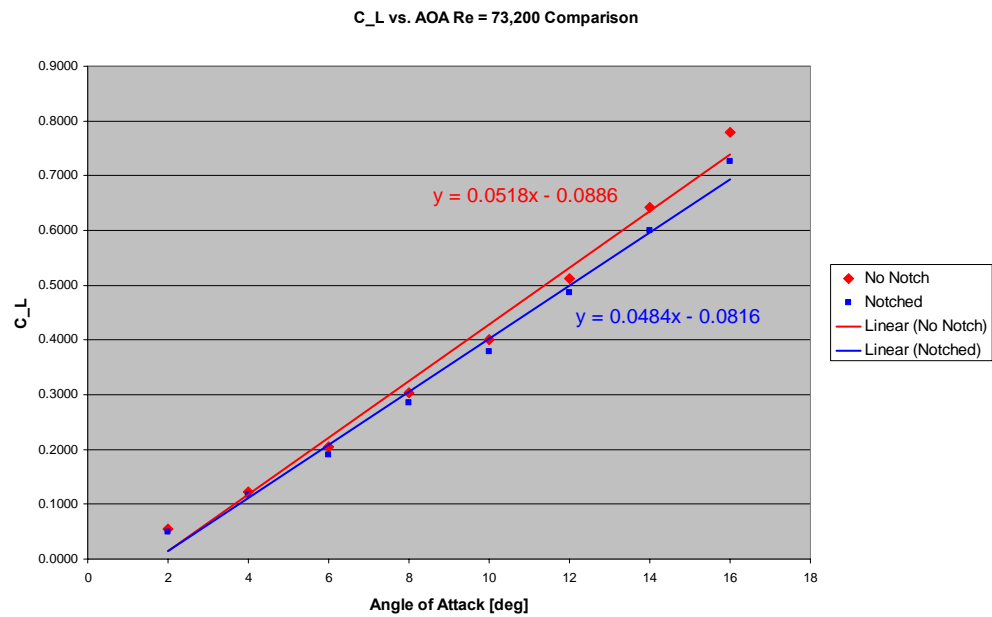


Figure 35: 3-D Coefficient of Lift vs. Angle of Attack for Notched/Unnotched–Re=73,200

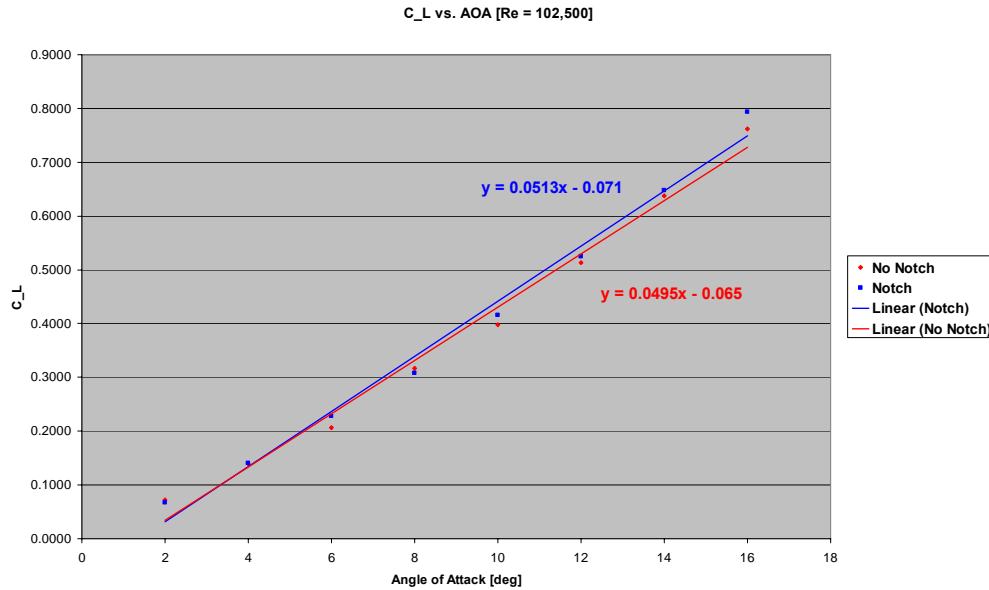


Figure 36: 3-D Coefficient of Lift vs. Angle of Attack for Notched/Unnotched–Re=102,600

As is observed in the preceding graphs the slope of the C_L vs. α curve decreases slightly for the notched configuration, with the exception of the $Re = 102,500$ case where the slopes are almost identical. This trend is most likely due to the reduction in lift force caused by the removal of planform area. Even though a reduction in planform area would tend to raise C_L values, apparently the reduction in lift force due to the smaller planform area, at the lower Reynolds numbers, has a dominant effect on the lift coefficient. While this reduction in lift coefficient slope might seem counter productive, we have not yet discussed the effects that the notches have on drag forces.

3.1.2: L/D vs. α

The lift coefficient isn't a particularly revealing performance parameter for wings. For this study it was mainly considered to check for consistency between our data and last year's data, as well as Thin Airfoil Theory. The lift over drag ratio brings the important forces, lift and drag, into comparison. Higher L/D values are desired as this means that a given wing at a given angle of attack is capable of producing more lift at a lower drag than another wing with a lower L/D.

Since a major goal of this study has been to see whether or not cutting notches into a wing at local lift peaks along the wing span will produce a more elliptical lift distribution (with

lower induced drag), the L/D comparisons between notch and no-notch plate configurations proved to be very useful in determining which setup performed more favorably.

For comparison reasons and time constraints we have focused only on the Reynolds number = 102,000 configuration:

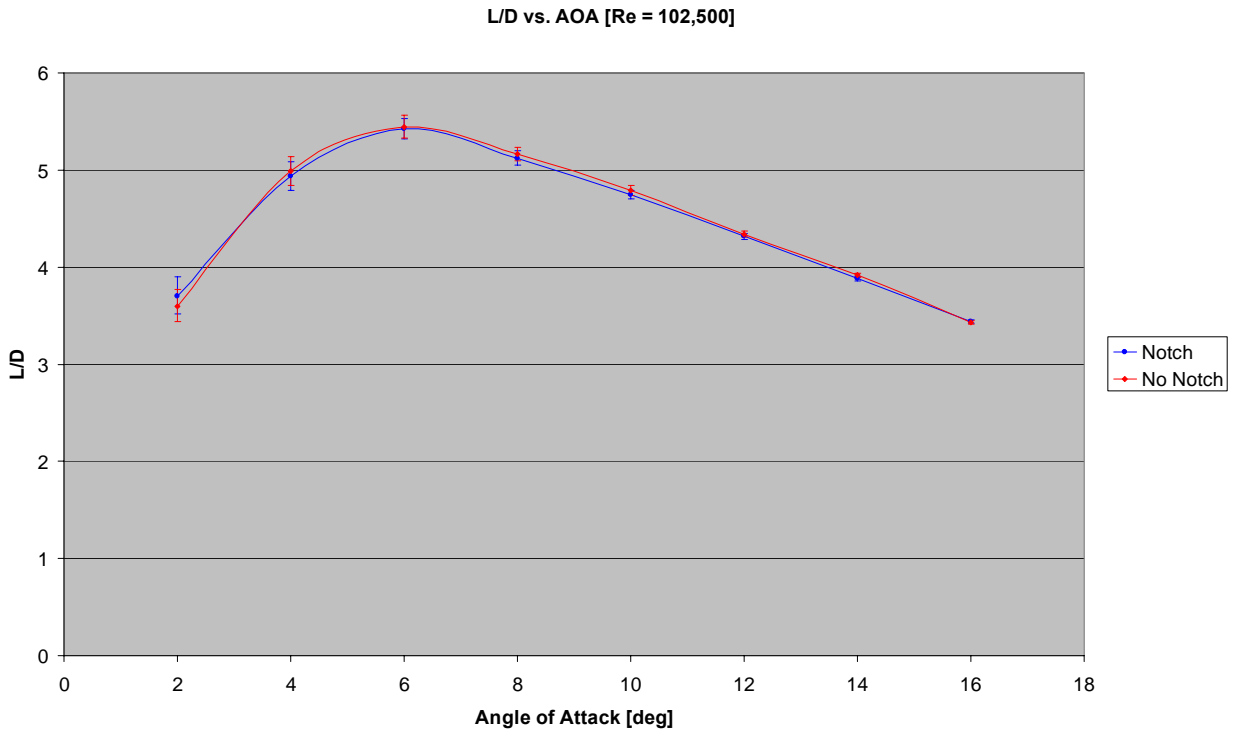


Figure 37: Notched/Unnotched Lift to Drag Comparison

As can be deduced from this plot, the performance of both wing configurations is *very* similar; however the no-notch configuration does slightly out-perform the notched configuration at peak L/D. The peak for both plates is at 6° angle of attack with L/Ds of 5.447 and 5.422 for the no-notch and notched setups respectively. Some overlap does exist between the error bars for all angles of attack bringing into question as to whether or not the no-notch configuration is indeed better. As stated, the performance differences between the setups is extremely small and therefore while it may appear that the no-notch configuration is better, the uncertainty with which this statement is made is moderately large.

We also decided to run comparisons to last year's data:

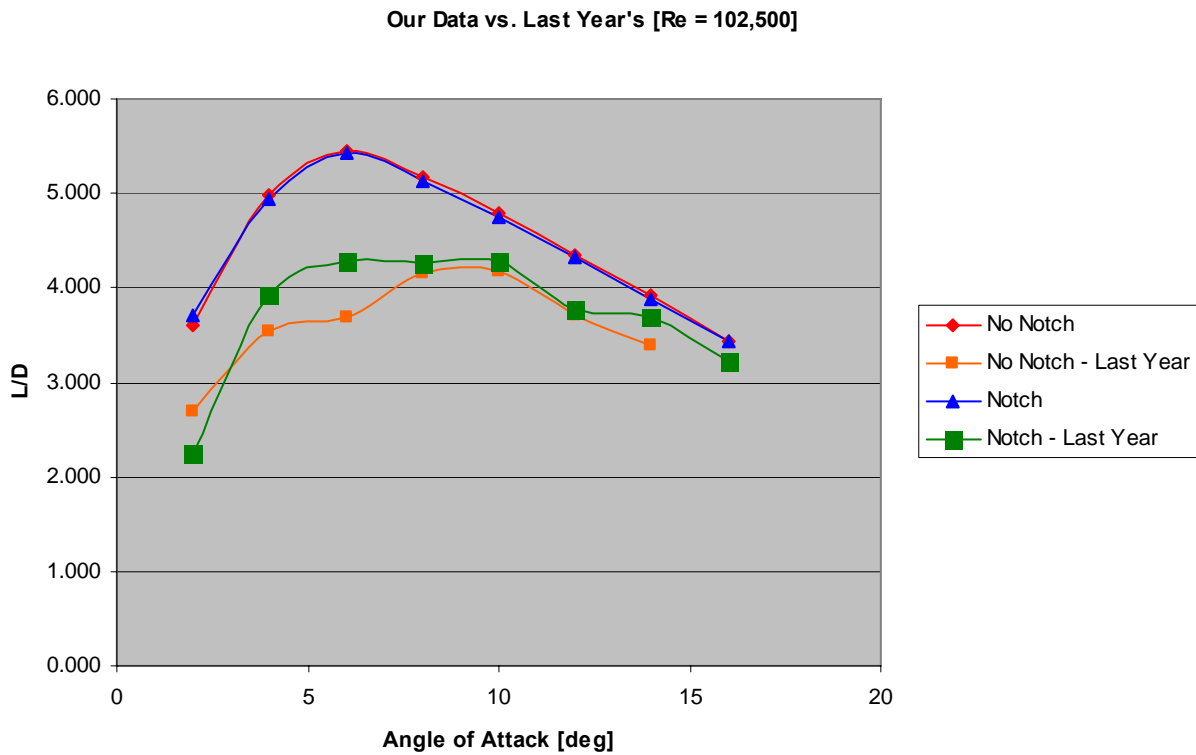


Figure 38: Lift to Drag Comparison to Previous Data

Our L/D values were higher than those found last year. Since our C_L curves matched closely to last year's data, we have determined that the difference must lie in the drag forces measured on the flat plates. Since we did not use the same force balance as last year's group (we had to replicate our own), and we used a newer, different proximeter, it is difficult to determine why our drag measurements were significantly different.

3.2: 2-D Test Results

3.2.1: C_L vs. α

To obtain “2-D” results for the plates, the endplate configuration was used. By placing endplates very close to the wingtips, the plates were “converted” to infinite wingspan airfoils. This new setup should greatly reflect the theory predicted by Thin Airfoil Theory, in that we expected the C_L vs. α slope would approach the predicted value: 2π for α in radiations or $.1097$ for α in degrees:

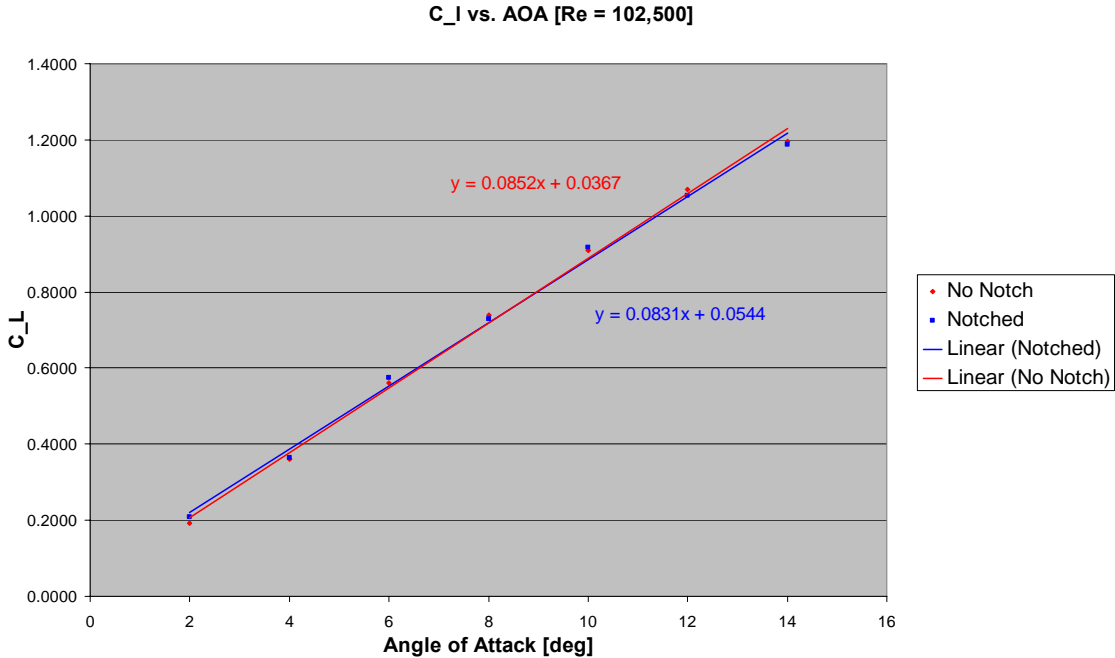


Figure 39: 2-D Coefficient of Lift vs. Angle of Attack

The notched configuration possessed a slightly lesser slope than that of the un-notched configuration. However the slopes are still considerably lower than the ideal value predicted by thin airfoil theory, ~ 0.027 lower. This is most likely due to the end plates not being close enough to the flat plates in order to fully eliminate the wingtip effects. Nevertheless the increase in slope is considerable when compared to the 3-D slopes which were ~ 0.50 .

3.2.2: L/D vs. α

For the 2-D L/D vs. α plot we expected to see an increase in the L/D curves and the same trends developed in the 3-D setup:

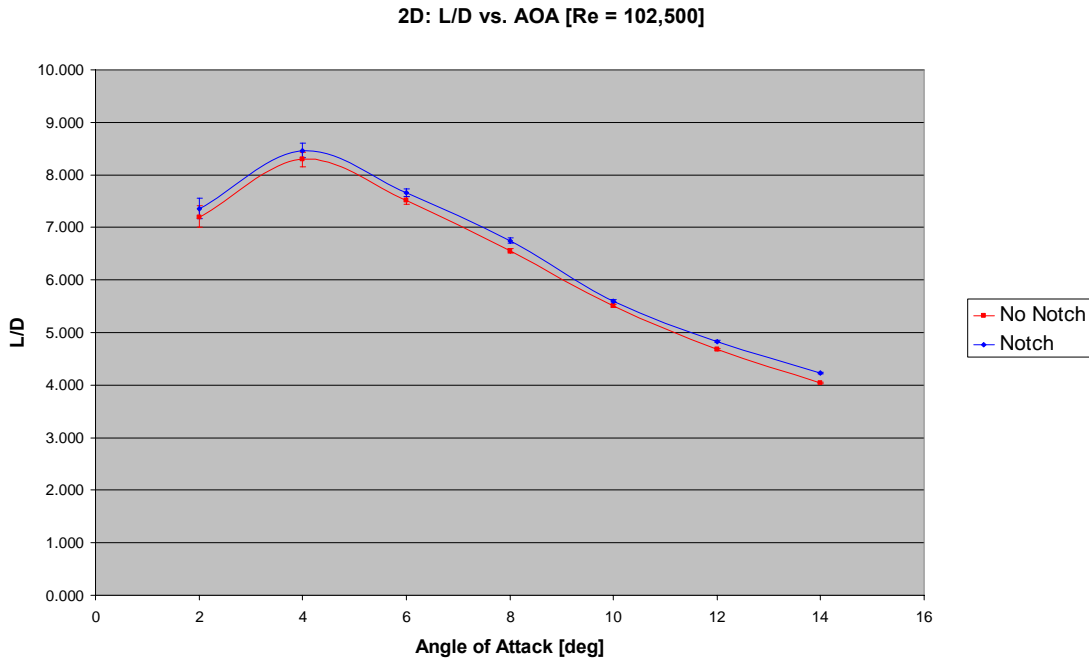


Figure 40: 2-D Lift to Drag Ratio

As seen from our data we in fact did not see the same trend as the 3-D scenario. In the 2-D endplate setup, the notched plate outperformed the un-notched plate.

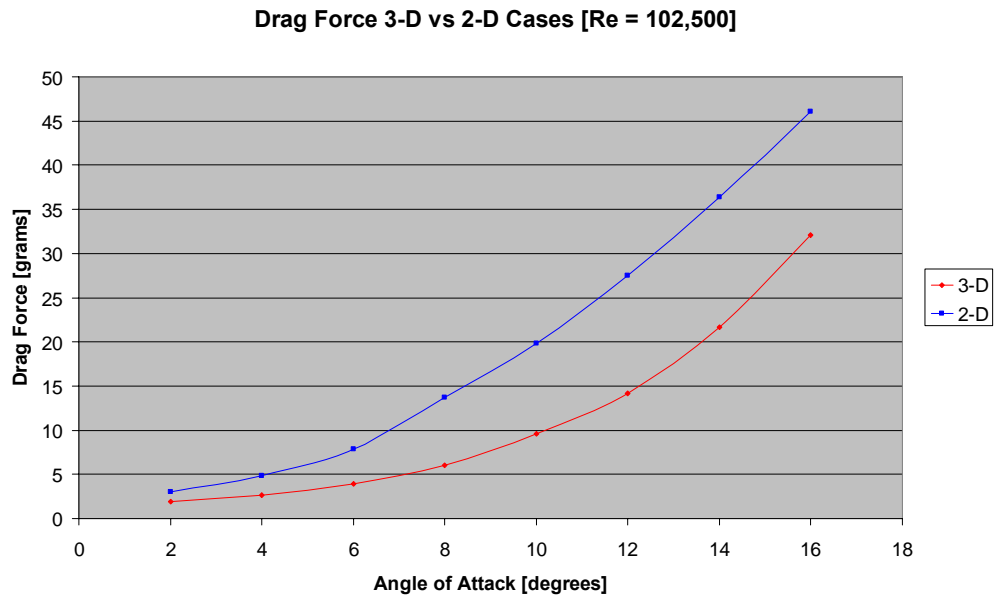


Figure 41: Drag Force 3-D vs. 2-D – Re=102,500

Another interesting fact to note was that the overall drag force increases in the 2-D setup as compared to the 3-D setup. While it might seem that the removal of wingtip-effects would have a reduction in drag, the contrary is actually true: it increases the drag. This is because the lift profile across the airfoil is essentially a constant value as opposed to the somewhat elliptical shape taken on during traditional 3-D tests. Since the lift is constant (and quite large, relatively) across the wingspan, more drag due to the lifting force occurs.

3.3: Induced Drag and Span Efficiency Factor

The drag on a 3-D wing is represented by the following equation:

$$C_D = C_{D_o} + KC_L^2 + \frac{C_L^2}{\pi(AR)e_s} \quad (11)$$

Or

$$C_D = C_{D_o} + \frac{C_L^2}{\pi(AR)e_o} \quad (12)$$

The terms e_o and e_s refer to the Oswald and span efficiencies respectively. The total induced drag on the wing can be represented as follows:

$$C_{D_I} = \frac{C_L^2}{\pi(AR)e_o} \quad (13)$$

For the ideal elliptically shaped lift profile, e_o and e_s are equal to one. For all non-ideal lift profiles, the value is less than one. Therefore, in order to minimize the amount of induced drag on a wing, one desires a span efficiency as close to one as possible. For purposes of this study, the span efficiency factor was focused on because it is more directly related to the elliptical lift profile than the Oswald efficiency which includes the term K . By defining the following expressions, we can determine the span efficiency e_s from the 2-D and 3-D C_D vs. C_L^2 data:

$K \equiv$ Slope of the 2-D C_D vs. C_L^2 Plot

$K_o \equiv$ Slope of the 3-D C_D vs. C_L^2 Plot

$$K_o = \frac{1}{\pi(AR)e_o} \quad (14)$$

Since the drag coefficient equation is a linear function of C_L^2 , experimental data points can be plotted for the 3-D and 2-D cases to determine K_0 and K :

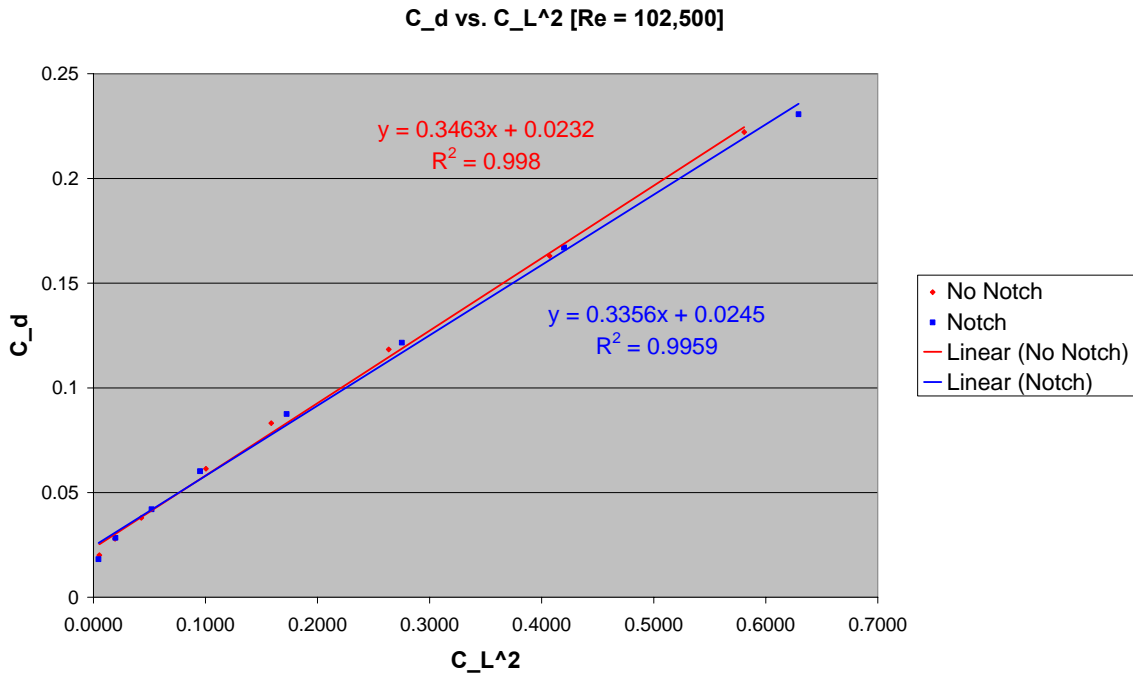


Figure 42: 3-D Coefficient of Drag vs. Square of Coefficient of Lift

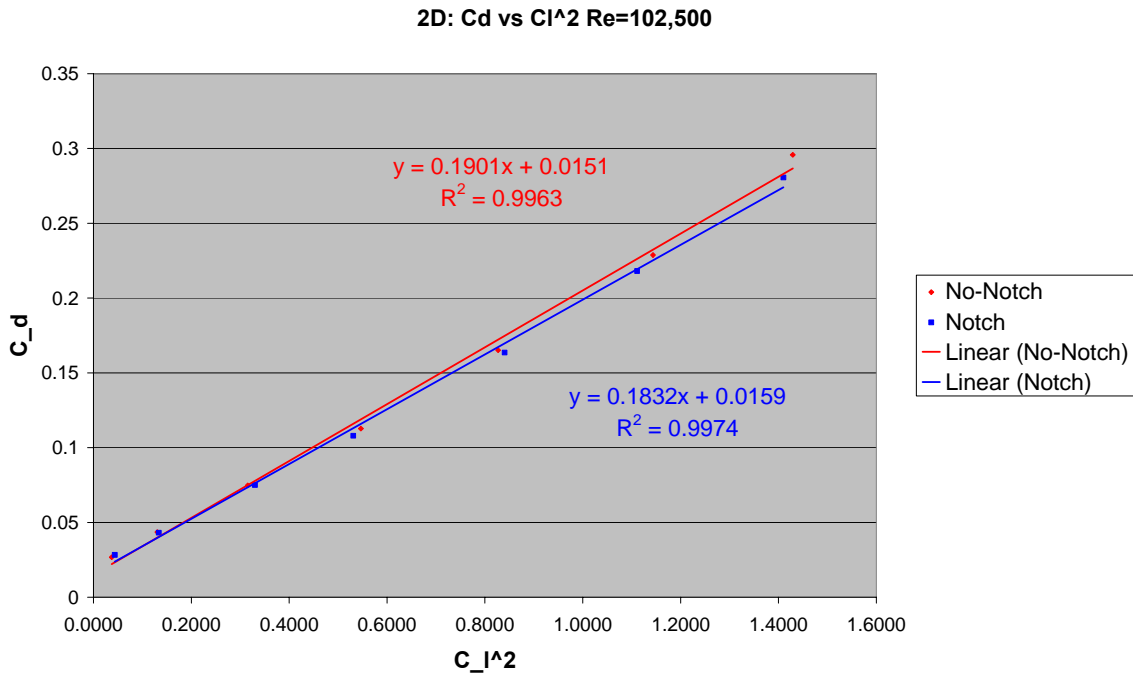


Figure 43: 2-D Coefficient of Drag vs. Square of Coefficient of Lift

Then by defining:

$$K_s = K_0 - K \quad (15)$$

And

$$e_s = \frac{1}{\pi(AR)K_s} \quad (16)$$

The span efficiency can be determined. Unfortunately, at the time of the writing of this report, the results are somewhat inconclusive. However preliminary analysis has shown that the notched configuration may have approximately 2.5% less induced drag than the un-notched setup. Therefore this is an important preliminary conclusion since we originally set out to determine whether or not notched wings could in fact reshape the span-wise lift profile to be more elliptical. A reduction in the induced drag suggests that this may in fact be the case.

3.4: Flight Test Results

Results from our flight tests did indeed match the phenomenon observed in the wind tunnel in that no significant change in velocity was observed between notched and unnotched flights. Using the film and known length of the lasso (11 feet) we were able to calculate velocities and compare them using the following equation:

$$V = \frac{2\pi R(\text{rev})}{t} \quad (17)$$

For the unnotched case the average velocity was calculated to be approximately 41 ft/s. Exposing the notched elevons yielded a velocity of 46 ft/s. This shows approximately a 10% difference in velocity between the two planforms. This test method is far from perfect however and there are many possible sources of error. Flying the aircraft until battery cutout with a fixed test rig or using a chronometer to establish velocity would be more direct methods however we did not have the resources or time to set up these flight tests. As a result our flight tests can lead us to deduce that the effect of trailing edge notches is small but we cannot be confident in that conclusion. More flight tests are required to be certain.

Table 2: Flight Test Data

Flight Test Data		
	Revolutions in 30 Seconds	Velocity Calculated (ft/s)
Notched	20	46
Not Notched	18	41

Section 4: Conclusions

The purpose of this project was to study the effects of trailing edge notches on an airfoil with an aspect ratio equal to one at low Reynolds numbers. More specifically the desired goals were to determine whether or not notches in the trailing edge significantly reduced induced drag on the airfoil as well as increase the overall lift over drag ratio. Furthermore there was a desire to compare the data collected from this study to a similar study conducted a year earlier and also apply notches to an actual cambered MAV to see if there were improvement in flight endurance and range.

This study concluded that there are no significant improvements in the L/D ratio when 1” triangular notches at the 60% half-span are applied to the trailing edge of a flat-plate wing. However, this study did calculate approximately a 3% decrease in induced drag when these notches were applied. Nevertheless, it is the opinion of this group that the small decrease in induced drag does not justify the use of trailing edge notches.

In comparison to the previous study there were significant contradictions. The previous study concluded that notches greatly improved the L/D ratio of airfoils with an aspect ratio of one at low Reynolds numbers. Also, as seen in Figure 36, the L/D ratios collected from this study were much higher than the ratios in the previous study. Possible explanations could be contributed to different equipment and different styles of wind tunnel testing.

Finally, this study concluded that trailing edge notches applied to a cambered MAV did not consistently or significantly improve nor hinder aircraft endurance or range. As there is a great deal of confidence in the validity of the data collected for this study, there is still a possibility that it does not fully prove that notches have no positive effect on flight performance of an MAV. As seen with the previous study, it was determined that notches did significantly improve L/D ratios leading to the need for further research on the subject.

References

- [1] McMichael, J. M., and Col. Francis, M. S., “Micro Air Vehicles – Toward a New Dimension in Flight,” Defense Advanced Research Projects Agency, TTO Document, Washington, DC, 7 Aug. 1997, URL: http://www.fas.org/irp/program/collect/docs/mav_auvsi.htm [cited 10 October 2006].
- [2] Goebel, Greg “Unmanned Aerial Vehicles,” URL: http://www.vectorsite.net/twuav_17.html [cited 10 October 2006].
- [3] Torres, G., and Mueller, T.J., “Aerodynamic Characteristics of Low Aspect Ratio Wings at Low Reynolds Number,” *Progress in Astronautics and Aeronautics*, Vol. 195, pp. 115-141, 2001.
- [4] Null, W., and Shkarayev, S., “Effect of Camber on the Aerodynamics of Adaptive-Wing Micro Air Vehicles” *Journal of Aircraft*, Vol. 42, No. 6, November-December 2005.
- [5] Kunz, P., and Kroo, I., “Analysis and Design of Airfoils at Ultra-Low Reynolds Numbers,” *Progress in Astronautics and Aeronautics*, Vol. 195, pp. 35-60, 2001.
- [6] Tucker, V.A., “Gliding Birds: Reduction of Induced Drag by Wing Tip Slots Between the Primary Feathers” Department of Zoology, Duke University, Durham, NC, 1993.
- [7] Drovetski, S. “Influence of the Trailing-Edge Notch on Flight Performance of Galliforms,” *The Auk*, Vol. 113, pp. 802-810, 1996
- [8] Ellington, C.P., and Usherwood, J.R., “Lift and Drag Characteristics of Rotary and Flapping Wings” University of Cambridge, Cambridge, England, 2001.
- [9] Blanchard, S., DeFusco, D., Donoghue, C., “Experiments on Trailing Edge Notches for Micro Air Vehicle Wings.” Worcester Polytechnic Institute, Worcester, MA, 2006.
- [10] http://images.military.com/pics/SoldierTech_WASP-1.jpg
- [11] Raymer, Daniel, “Aircraft Design: A Conceptual Approach” American Institute of Aeronautics and Astronautics Inc., Reston VA, 1999
- [12] Blondin, S.M, De Barros, I.A, Falcone, M.F, Henry, D.B, McWilliams, K.J, Seney, S.D, Wong, J, Olinger, D.J, “Design of a Micro Air Vehicle” *MQP WPI* 2001

Appendix A – Force Balance Construction

A.1: Base Construction

80/20 Aluminum T-Slot

Website: www.8020.net

Online Vendor Website: www.airincorporated.com

Part Dimensions

- Inch Profile 1" x 1" x 97", Item #1010 x 97"
- (40) Bolt Assembly (includes screw and nut), $\frac{1}{4}$ "(thread diameter), 20 (thread count), $\frac{1}{2}$ " (length), Item #3491
- (4) 3-Holed Joining Strips, Item #4118
- (12) 2-Hole Inside Corner Bracket, Item #4119

T-Slot Cut Dimensions

- (4) 5" pieces
- (4) 11" pieces
- (4) 5 $\frac{1}{2}$ " pieces
- (4) 2" pieces

The aluminum cutting was performed with a band-saw in Washburn Shop. In terms of the finish of the cut, it's recommend using a band-saw with as "fine" of teeth as possible. It became evident that the larger toothed band-saw we used for the pieces that were >2" left uneven surfaces that required filing and hammering in order to assure that all pieces fit together and sat perpendicular to adjacent pieces. In addition to the cutting and finishing operations, the 5 $\frac{1}{2}$ " pieces were threaded ($\frac{1}{4}$ " 20 threads) so that joining plates could be screwed into them.

With the materials cut to size, the force balance base was assembled (see pictures in Section 2.1 or current force balance for example of how the pieces should be oriented). No welding was necessary. The T-Slot Aluminum allowed for all construction to be completed with screw and nut. The overall dimensions are H: 5 $\frac{3}{4}$ ", L: 11", W: 6" (length and width measured from joining plates).

A.2: Steel Shim Construction

Steel Shim Stock

Website: www.mscdirect.com

Part Dimensions

- Steel Shim Stock, 0.0015" (thickness), 6" (width), 100" (length), Item # 00049999

T-Slot Cut Dimensions

- (4) 3.5" x 1"

The steel shim was thin enough to be cut using metal hand shears. Once cut to the right size, the four shim pieces were attached to the force balance base and stand base, two to the front of the stand base and two to the back. Each shim piece had three holes drilled into them, two for the stand base and one for the force balance base.

Appendix B – Stand and Sting CAD Design

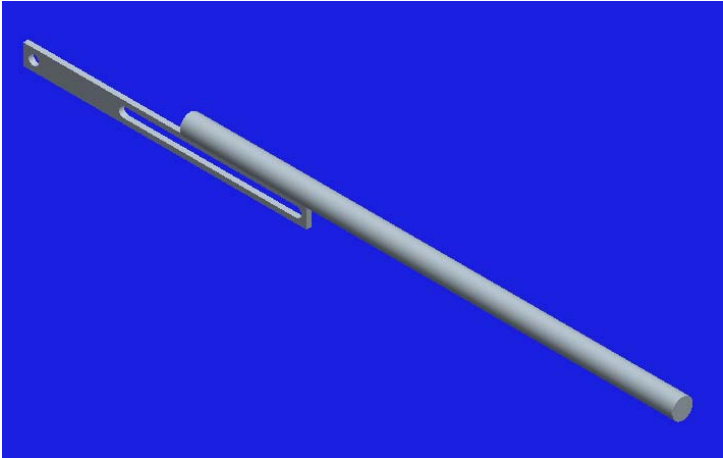


Figure 44: Sting [8]

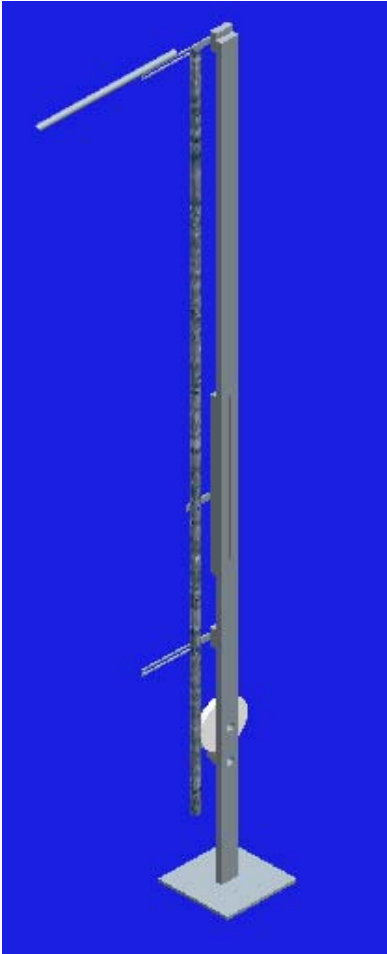


Figure 45: Stand and Sting [8]